HYDROLOGICAL PROCESSES
Hydrol. Process. (2013)
Published online in Wiley Online Library
(wileyonlinelibrary.com) DOI: 10.1002/hyp.9909

Modelling how vegetation cover affects climate change impacts on streamflow timing and magnitude in the snowmelt-dominated upper Tuolumne Basin, Sierra Nevada

Nicoleta C. Cristea,[1]* Jessica D. Lundquist,[1] Steven P. Loheide II,[2] Christopher S. Lowry[3] and Courtney E. Moore[1]

[1] *Civil and Environmental Engineering, University of Washington, Seattle, WA, USA*
[2] *Civil and Environmental Engineering, University of Wisconsin-Madison, Madison, WI, USA*
[3] *Geology, University at Buffalo, Buffalo, NY, USA*

Abstract:

We investigated, through hydrologic modelling, the impact of the extent and density of canopy cover on streamflow timing and on the magnitude of peak and late summer flows in the upper Tuolumne basin (2600–4000 m) of the Sierra Nevada, California, under current and warmer temperatures. We used the Distributed Hydrology Soil Vegetation Model for the hydrologic modelling of the basin, assuming four vegetation scenarios: current forest (partial cover, 80% density), all forest (uniform coverage, 80% density), all barren (no forest) and thinned forest (partial cover, 40% density) for a medium-high emissions scenario causing a 3.9 °C warming over a 100-year period (2001–2100). Significant advances in streamflow timing, quantified as the centre of mass (COM) of over 1 month were projected for all vegetation scenarios. However, the COM advances faster with increased forest coverage. For example, when forest covered the entire area, the COM occurred on average 12 days earlier compared with the current forest coverage, with the rate of advance higher by about 0.06 days year^{-1} over 100 years and with peak and late summer flows lower by about 20% and 27%, respectively. Examination of modelled changes in energy balance components at forested and barren sites as temperatures rise indicated that increases in net longwave radiation are higher in the forest case and have a higher contribution to melting earlier in the calendar year when shortwave radiation is a smaller fraction of the energy budget. These increases contributed to increased midwinter melt under the forest at temperatures above freezing, causing decreases in total accumulation and higher winter and early spring melt rates. These results highlight the importance of carefully considering the combined impacts of changing forest cover and climate on downstream water supply and mountain ecosystems. Copyright © 2013 John Wiley & Sons, Ltd.

KEY WORDS hydrologic modelling; climate change; vegetation cover; streamflow timing; streamflow changes; snowmelt

Received 20 September 2012; Accepted 14 May 2013

INTRODUCTION

Mean timing of snowmelt run-off has advanced by approximately 1–3 weeks in many mountainous catchments across western North America (Regonda *et al.*, 2005; Stewart *et al.*, 2005). This trend towards earlier snowmelt and earlier streamflow timing has been attributed to the broad-scale increase of winter and spring temperatures by about 1–3 °C over the past 50 years (Stewart et al., 2005). These changes appeared to be sensitive to the effects of increased air temperature, primarily in basins below about 2500 m (Regonda *et al.*, 2005), and are expected to continue in the future, because of anticipated climate change effects (Hamlet and Lettenmaier, 1999; Leung and Wigmosta, 1999; Leung *et al.*, 2004).

In addition to climate, vegetation cover type and extent also affect streamflow patterns (Jones and Post, 2004), and watershed managers have options in how they choose to manage the vegetation cover to control streamflow patterns (Grant *et al.*, 2008). Therefore, the role vegetation plays in the magnitude of these changes in a warming climate is of interest. Forests interact with snow through altering its spatial distribution and energy exchanges with the environment. Forests reduce ground-level incoming shortwave radiation while increasing longwave radiation (Hardy *et al.*, 2004; Link *et al.*, 2004; Boon, 2009) and reduce turbulent energy transfer at the snow surface (Hardy *et al.*, 1997). The absence of vegetation causes snow accumulation and melt rates to increase and evapotranspiration to decrease (Whitaker *et al.*, 2002). Melt rates were found generally to be higher

*Correspondence to: Nicoleta C. Cristea, Civil and Environmental Engineering, University of Washington, 159 Wilcox Hall, Box 352700, Seattle, WA 98195-2700, USA
E-mail: cristn@u.washington.edu

in barren areas than under the forest in Canada (Winkler *et al*., 2005; Boon, 2009; Burles and Boon, 2011). However, differential snowmelt rates between the barren regions and the forest may vary with elevation. At lower elevation (1435 m), snowmelt rates in Canadian forests were lower than in the clear-cut areas, whereas at higher elevation (1650 and 1781 m), snowmelt rates of forested and barren areas approached equality (Whitaker *et al*., 2002). At temperatures above freezing, melt rates were higher under the forest, but at near-freezing temperatures, melt rates in the barren areas were higher in the central Pyrenees; these differences were attributed to increased net longwave radiation at temperatures above 0 °C and to the lower albedo under the forest (Lopez-Moreno and Latron, 2008).

The effects of vegetation changes on streamflow have long been investigated because of their economical and ecological importance. Historically, paired watershed experiments have evaluated forest harvesting effects on flows typically at relatively small spatial scales of less than 10 km^2 (Hewlett, 1971; Hewlett, 1982; Robinson *et al*., 2003; Andreassian, 2004; Jones and Post, 2004; Grant *et al*., 2008). In general, changes in streamflow as a result of vegetation disturbance varied with the nature of basin, vegetation type, elevation and climate, but in most cases, higher peak flows have been reported in the clear-cut basins compared with control vegetated basins as a result of vegetation removal. More recently, in addition to paired watershed studies, hydrologic modelling has been used as a means of identifying changes in the magnitude and frequency of peak flows in response to vegetation cover changes (e.g. Schnorbus and Alila, 2004; Alila *et al*., 2009; Cuo *et al*., 2009, 2011; Kuraś *et al*., 2012).

Hydrologic modelling allows for comparisons of streamflow time series generated assuming different land cover scenarios, while maintaining the same climatic and precipitation patterns (same model forcing data). Examples of such modelling experiments are described in Schnorbus and Alila (2004) and Kuraś *et al*. (2012) on catchments of 26 and 4.74 km^2, respectively, located in British Columbia, Canada. In these studies, partial or total removal of forest canopies was found to increase both the magnitude and frequency of annual peak discharge. Use of modelling experiments has the drawback of dealing with uncertainty in model representation of hydrologic processes, as well as issues related to model parameterization and the need for reliable streamflow and distributed internal states data to ensure that the model adequately represents the basin hydrology (Kuraś *et al*., 2011). However, the modelling approach allows for investigating hydrologic changes determined by both land cover and climate over many locations, periods and basin sizes (e.g. Cuo *et al*., 2009, 2011 on basins ranging 178–8316 km^2).

Here, we use hydrologic modelling to explore the role of vegetation on streamflow timing and magnitude under a warming climate for the upper Tuolumne River basin of the Sierra Nevada, California. The regional hydrology is very important for California water, as part of the Tuolumne River snowmelt is stored in the downstream Hetch Hetchy reservoir, which is a major component of the San Francisco water supply system. The timing of snowmelt and the amount of water available are therefore of great interest for resource managers concerned with hydropower production and with water supply for agricultural, urban and industrial use. Previous studies of Sierra Nevada basins have shown that streamflow timing will likely occur earlier as a result of climate change, leading to longer periods of lower flows during the summer, when water is most needed (Maurer, 2007; Null *et al*., 2010). These prolonged low flow conditions are detrimental not only for downstream water supply but also to the region's mountain ecosystems (Lowry *et al*., 2010, 2011). The upper Tuolumne River basin drains to Tuolumne Meadows, which has been designated as a place of outstanding scenic value by the National Park Service (NPS), which requires long-term conservation plans. Here, meadow vegetation and potential associated restoration strategies are intimately tied to local stream hydrographs, which in turn, are controlled by integrated processes across their contributing watershed (Loheide and Lundquist, 2009; Loheide *et al*., 2009; Lowry *et al*., 2011). These issues are representative of those addressed in mountainous basins across the western USA and British Columbia.

In this study, we use the Distributed Hydrology Soil Vegetation Model (DHSVM; Wigmosta *et al*., 1994) to simulate historic and projected future streamflows and additionally to explore how the vegetation cover influences streamflow timing and magnitude. Within the model, we create virtual experiments by specifying different vegetation scenarios to emulate paired watershed experiments, while applying the same future meteorology from a medium-high emissions scenario, A2 (IPCC, Intergovernmental Panel on Climate Change, 2001) of the Geophysical Fluid Dynamics Laboratory (GFDL) CM2.1 model of 3.9 °C warming. These scenarios were designed to evaluate the response of the hydrologic system to changes in climate as a function of forest cover without including a dynamic vegetation model or modelling explicitly forest change across space and time. The DHSVM explicitly models the effects of shading and vegetation cover and has previously been applied to evaluate effects on streamflow patterns from climate change (Leung and Wigmosta, 1999; Battin *et al*., 2007; Wiley and Palmer, 2008) and forest harvesting (Whitaker *et al*., 2002; Schnorbus and Alila, 2004; Kuraś *et al*., 2012). In a review of hydrologic models for applications

studying forest management and climate change, the DHSVM was identified to be the most suitable model to address questions related to forest effects on streamflow because of its high complexity and capability to represent forest processes in mountainous terrain (Beckers *et al.*, 2009). The main purpose of this analysis is to determine how land cover affects basin sensitivity to climate change (i.e. is a forested basin more or less sensitive to warming than a barren basin?).

STUDY SITE AND DATA SOURCES

The upper Tuolumne basin, located in Yosemite National Park in the Sierra Nevada of California, is a high elevation basin, ranging from 2600 to 4000 m a.s.l. (Figure 1). Its area of 186 km^2 comprises about 16% of the downstream Hetch Hetchy reservoir's drainage area. The underlying soils are thin (typically less than 1 m deep) and are derived from low permeability intrusive rocks (granodiorite), which erode slowly and interact little with streamflow (Huber, 1987). The basin is covered at lower elevations by dense forest (*Pinus contorta*, 39% of the total basin area) and by herbaceous meadow vegetation (meadow, 36%) and is barren (granitic bedrock, 24%) at higher elevations (Figure 1). Most of the forest-covered areas are located below the mean elevation of the basin (3200 m) as shown in Figure 1. High elevation, complex topography and low infiltration make the system snowmelt dominated. The climate is Mediterranean, with cold and wet winters and warm and dry summers. Over 80–90% of annual precipitation (800–1000 mm) falls as snow primarily during the winter, but there is significant seasonal and interannual variability in precipitation (Epke *et al.*, 2010). Middle elevations (2100–3000 m) and high elevations (above 3000 m) produce 40–60% and 30–40% of the annual snowmelt, respectively, in the larger Tuolumne basin (Rice *et al.*, 2011).

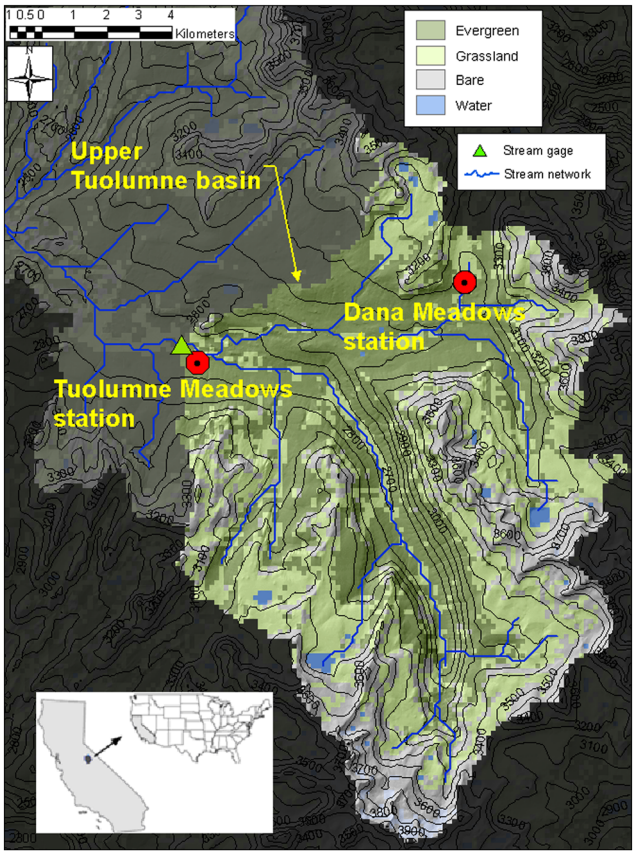

Figure 1. Upper Tuolumne basin, Sierra Nevada, California

Streamflow data were collected as part of the Yosemite Hydroclimate Monitoring Project beginning in August of 2001 (Lundquist *et al.*, 2003, 2004). Stream stage was measured with Solinst Levelogger© pressure transducers every half-hour at the location shown as a solid triangle in Figure 1, and both stream stage and discharge were manually measured once a week during the summer season. Observed stream stage time series were transformed into streamflow using rating curves relating water level to discharge calculated from manual measurements (Rantz *et al.*, 1982).

The 2003–2009 period used for model calibration experienced a relatively large range of climate conditions and hydrologic variability, which is representative of the region. An analysis of the long-term historic streamflow record (1916–2009) in the neighbouring Merced basin [United States Geological Survey (USGS) gage 11264500], which has similar climate, geology and vegetation cover as Tuolumne, showed that the 2003–2009 period encompassed conditions ranging between the ninth percentile (2007, the driest year) and 95th percentile (2006, the wettest year). Meteorological data were obtained from the Dana Meadows (37.9°N, 119.3°W, 2966 m) and Tuolumne Meadows (37.6°N, 119.7°W, 2600 m) snow pillow sites (Figure 1), which are managed by the California Department of Water Resources.

We chose the upper Tuolumne area as a case study for this investigation because (i) it is a high-elevation basin important for providing snowmelt water during the critical summer low flow conditions, (ii) the basin has a simple geology and is sensitive to changes in climate (Maurer, 2007) and (iii) forest cover manipulation was identified as a means to increase snow retention in other high-elevation regions of the Sierra Nevada (e.g. Bales *et al.*, 2011b). Streamflow series derived from four different vegetation scenarios and the same climate scenario from the GFDL CM2.1 model (3.9 °C warming) were analysed for changes in timing, peak magnitude and frequency, and summer low flow magnitude and frequency.

HYDROLOGIC MODELLING, CLIMATE DATA AND METHODS FOR STREAMFLOW ANALYSIS

Hydrologic model description and model set-up

The DHSVM calculates the full surface energy balance independently at each model grid cell, including terrain shading effects, radiation attenuation, wind modification and snow-canopy processes (Wigmosta *et al.*, 1994; Storck, 2000; Storck *et al.*, 2002). The DHSVM represents the seasonal snowpack as a two-layer system and solves the full surface energy balance at each time step. The surface (top) layer actively exchanges energy and mass with the atmosphere. The pack (bottom) layer acts as a mass and energy reservoir and exchanges inputs of heat and melt water with the surface layer.

Vegetation is represented in DHSVM as a two-level coverage, with the overstory covering a specified fraction of the pixel, typically the canopy closure, and an understory. Interception is modelled as a function of total snow and snow interception efficiency, until a maximum value, defined as the maximum interception capacity of that specific canopy type, is reached. Intercepted snow is subject to sublimation, mass release from the canopy (added to the ground snowpack) and melt (estimated through an energy balance equation). Evapotranspiration is represented by the Penman–Montieth approach (Shuttleworth, 1992), assumed to occur at the potential rate from wet surfaces and dependent on the soil moisture under unsaturated conditions. Calculations of evapotranspiration are based on weather variables, aerodynamic resistance (dependent on the wind velocity profile and vegetation characteristics) and canopy resistance (dependent on temperature, vapour pressure deficit, photosynthetically active radiation and soil moisture). Above the overstory, a logarithmic (flat plate boundary) wind profile is assumed, whereas through the overstory and understory, wind decreases exponentially until it meets a new (lower velocity) logarithmic profile near the surface (Wigmosta *et al.*, 1994). The DHSVM simulates overland flow and both saturated and unsaturated subsurface flow. Streamflow is routed through a network in which each stream section is treated as a linear reservoir using a Muskingum–Cunge algorithm. Model equations representing the snowpack energy balance are given in Appendix A. Additional model details and conceptualization of hydrologic processes and model equations are described in Wigmosta *et al.* (1994, 2002) and summarized in several subsequent studies in which the DHSVM was used (e.g. Thyer *et al.*, 2004; Jost *et al.*, 2009 or Bewley *et al.*, 2010).

For the upper Tuolumne basin, the DHSVM was run at a 3-h time step with a 150-m grid resolution. This resolution was chosen to best resolve the stream networks and water transfers between grid cells, while remaining coarse enough to maintain computational efficiency. Spatial inputs of elevation, vegetation, soil type and depth, geology and terrain shading were pre-processed from available NPS and USGS datasets. Temperature was distributed across the basin with a constant lapse rate of $-6.5\,^{\circ}\mathrm{C\,km^{-1}}$, which was the average found from a distributed network of over 40 sensors in this region (Lundquist and Cayan, 2007). Precipitation was distributed using relative weighting derived from maps of monthly climate normal precipitation from the Parameter-elevation Regressions on Independent Slopes Model (PRISM; Daly *et al.*, 1994, 2002, 2008). Forest coverage (39% of the watershed area, spatial extent shown in Figure 1) was represented as a single class (conifers, predominantly lodgepole pine *P. contorta*) of uniform 80% fractional coverage (of the pixel). Vegetation parameters have been established on the basis of data from personal communications with park managers and from the literature, primarily from studies that applied the DHSVM at sites where lodgepole pine forests were present (e.g. Thyer *et al.*, 2004; Bewley *et al.*, 2010). Model parameters are given in Table A1, Appendix A.

Temperature, relative humidity, incoming shortwave radiation and wind speed data used for calibrating the model for years 2003–2009 were recorded at Dana Meadows (Figure 1). Because the precipitation data record at this station was affected by instrument failure during 2006–2009, we used precipitation measured at Tuolumne Meadows (Figure 1), which was scaled by a factor of 1.3 to match the Dana Meadows records (based on total precipitation) and to represent the different PRISM precipitation weights between these two stations. The factor of 1.3 matched the ratio of the two stations during the years of overlap. The air temperature lapse rate ($-6.5\,^{\circ}\mathrm{C\,km^{-1}}$) was checked through lapsing the air temperature recorded at Tuolumne Meadows and comparing it with air temperature recorded at Dana Meadows. This comparison revealed a relatively uniform scatter around the 1 : 1 line and indicated that this lapse rate is suitable for representing air temperature distribution across the upper Tuolumne basin. In addition to this comparison, and given the importance of varying temperature with elevation, we also examined the model's sensitivity to constant lapse rates of -4.5 and $-8.5\,^{\circ}\mathrm{C\,km^{-1}}$, relative to the base case of $-6.5\,^{\circ}\mathrm{C\,km^{-1}}$. Although variations in lapse rates have been found to affect basin hydrology in other basins (e.g. Minder *et al.*, 2010), varying the lapse rate had little effect on streamflow in our study area because the overall elevation range in the basin is relatively small and the forcing temperature (2966 m) is located near the middle of the overall range (Figure 1). The $-8.5/-4.5\,^{\circ}\mathrm{C\,km^{-1}}$ lapse rate resulted in slight increase/decrease in late-season discharge and a shift of ± 2 days in centre of mass, COM (as in Stewart *et al.*, 2005, the date on which fractional cumulative discharge

reaches 50%). Therefore, we kept the lapse rate constant at $-6.5\,^{\circ}\mathrm{C\,km^{-1}}$, which was found to represent temperature variations with elevation for all further simulations.

Incoming shortwave radiation was distributed using solar geometry calculations, then corrected for terrain shading effects using monthly maps of terrain shadowing constructed using the solar geometry from day 15 of each month (Wigmosta *et al*., 1994). Soil saturated hydraulic conductivity values were estimated using the USDA soil classifications (U.S. Department of Agriculture, Natural Resources Conservation Service, 2006) and mean saturated conductivity values provided by Carsel and Parrish (1988) for each soil class (Table A1, Appendix A). During preliminary sensitivity tests, these were varied by one order of magnitude (both higher and lower), but model results were relatively insensitive to these variations. Soil depths were checked during field visits and found to be less than 1 m in most locations and less than 3 m in most meadow locations, which is consistent with reported values (U.S. Department of Agriculture, Natural Resources Conservation Service, 2006) and those used in DHSVM (Lowry *et al*., 2010). Forest parameters were set to 80% fractional coverage, 5.0 leaf area index (LAI) and 30% radiation attenuation (k, Equation (A5), Appendix A) based on park vegetation surveys, discussions with park foresters and values reported in the literature (Table A1, Appendix A). Additional discussion of model parameter sensitivity is provided in Appendix A.

The DHSVM has no explicit representation of either wind-driven or gravity-driven snow redistribution processes, which are dominant sources of spatial variability in snow accumulation in mountain basins, and show a strong spatial linkage to terrain features. Each of these processes tends to deposit snow in topographically concave locations, at the head of cirques and in the lee of terrain barriers. The wind speed measured at the weather station was used at all grid cells, a simplifying assumption that obviates the computational cost of a dynamical wind model. The data and methods needed to distribute wind speed across the basin (see, e.g. Liston and Elder, 2006; Winstral *et al*., 2002; Winstral *et al*., 2009) are beyond the scope of this work and represent a potential future improvement. The Tuolumne Basin is a maritime snowpack, where falling snow is wetter and denser than that in continental regions where most snow redistribution studies have taken place. Therefore, snow deposition is assumed to be more a function of precipitation intensity (accounted for here by PRISM maps) and not a function of wind redistribution. Annual average measured wind speeds are relatively small, less than $1.5\,\mathrm{m\,s^{-1}}$. Marks and Dozier (1992) found that in the Sierra Nevada, sublimation and evaporation can account for a reduction of up to 20% of the snow mass; however, they note that energy from net radiation was five to ten times greater than all other forms of heat transfer combined. Thus, it is reasonable for this application to give radiation distribution a higher priority and to assume the station wind measurements are homogenous over the domain.

The stream network was developed from a hydrologically conditioned 150-m digital elevation model (DEM); small (1–3 m) adjustments to individual elevation pixels were made to force the derived stream network to match the NPS stream map, which was developed from site surveys. These adjustments were necessary because some streams in the area are routed via incised bedrock channels that are not represented on a 150-m DEM. Modelled streamflow was routed at each time step using the stream channel network, with each stream section treated as a linear reservoir. Water also entered the channel via overland flow and saturated subsurface flow in the soil layers. Because the majority of the basin is made up of intrusive igneous granodiorite, modelled influences from deep groundwater were negligible.

Climate data and model scenarios

To explore potential changes in the basin hydrology as a result of increasing temperature and as a function of vegetation cover, we performed two types of simulations. First, we ran model sensitivity tests to changes in temperature (ΔT tests) on the historical record and then we used long-term climate data (2001–2100, 3.9 °C warming) based on output from Geophysical Fluid Dynamics Laboratory (GFDL) CM2.1 model (Delworth *et al*., 2006; Knutson *et al*., 2006; Stouffer *et al*., 2006). For the ΔT sensitivity tests, we considered the two extreme vegetation scenarios, forest and barren, for the historic 2003–2009 period. The temperature was raised by $\Delta T = 3\,^{\circ}\mathrm{C}$ in the forcing dataset, and the results were compared with the simulations run using the historic meteorology. This ΔT was chosen to represent the approximate temperature increase by the last decades of the century in the GFDL scenario. The purpose of running the ΔT sensitivity tests (model scenarios 1–4, Table I) was to allow comparisons of the energy balance components, snow water equivalent (SWE) and streamflow between forested and barren cases for the historic temperature T and

Table I. DHSVM scenarios for ΔT sensitivity tests

Scenario	Vegetation cover	Scenario assumption
1	All forest	Historic T
2	All forest	Historic $T + 3\,^{\circ}\mathrm{C}$
3	Barren	Historic T
4	Barren	Historic $T + 3\,^{\circ}\mathrm{C}$

increased, historic $T+3\,^{\circ}C$ forcing data, while holding all other variables (e.g. precipitation) constant.

The climate scenario is a medium-high emissions scenario (A2) from the GFDL model (3.9 °C warming) that assumes emissions increase continuously to near $30\,Gt\,yr^{-1}$ by 2100 (IPCC, Intergovernmental Panel on Climate Change, 2001). This scenario was chosen to be compatible with other climate impacts studies in the region and was identified as appropriately representing plausible future conditions in California (e.g. Maurer, 2007; Cayan *et al*., 2008). We initially considered a range of four climate scenarios based on the Parallel Climate Model (PCM; Washington *et al*., 2000; Meehl *et al*., 2003) and GFDL CM2.1 models' output for both B1 and A2 IPCC scenarios for a range of projected temperature increases ranging from 1.7 (PCM B1) to 3.9 °C (GFDL A2) following Cayan *et al*. (2008). Although exact numbers vary, the qualitative nature of the impacts was the same across scenarios. For clarity, we chose the A2 GFDL scenario to illustrate the findings for this study.

Downscaled climate data for the A2 GFDL scenario for the 2001–2100 period (daily minimum and maximum temperature and daily precipitation) were retrieved from http://tenaya.ucsd.edu/wawona-m/downscaled, where a data collection representing future climate scenarios was made available as part of USGS Computational Assessments Scenarios of Change for the Delta Ecosystems project. The downscaling procedure of transforming the coarse resolution information from the A2 GFDL model ($2.5^{\circ} \times 2.5^{\circ}$) to a finer resolution ($1/8^{\circ} \times 1/8^{\circ}$) followed the method of constructed analogues described in Hidalgo *et al*. (2008).

For the Tuolumne area, the 1/8° cell closest to the Dana Meadows station was selected for the climate data. Because a difference of about 140 m existed between the mean elevation of this cell and the Dana Meadows elevation, we bias-corrected the projected climate dataset for differences in temperature and precipitation. Monthly biases in air temperature and precipitation were estimated on the basis of the climate model output averaged over the 1971–2000 historic period and PRISM averages for the same period. Air temperature was corrected using these monthly biases, and precipitation was scaled by a factor of 1.2 (the mean 1971–2000 bias) for the entire 2001–2100 period. The total projected annual precipitation and annual average temperature for the climate change scenario are shown in Figure 2. Although there was no quantified trend in precipitation, the last two decades were drier than the average, with total average precipitation about 8% less than during the historic period and a significant increase in air temperature of about 3.9 °C by the end of the century (Figure 2).

Once the climate input data were established, we set up DHSVM to simulate streamflows for the 2001–2100

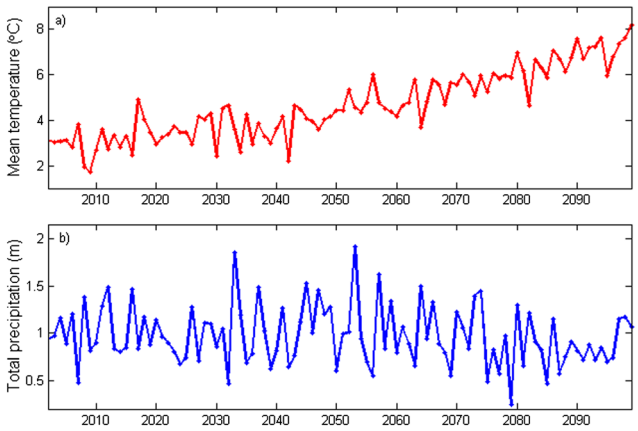

Figure 2. a) Mean annual temperatures and b) total annual precipitation for the climate simulation period 2001–2100

period assuming four different vegetation scenarios: (1) current forest, spatially distributed on the extent shown in Figure 1, as the base case; (2) entire basin covered by forest; (3) entire basin is barren and (4) current forest extent, but fractional coverage is reduced, presumably as a result of thinning or controlled fire. The four vegetation scenarios are summarized in Table II. These scenarios were considered to explore the basin sensitivity to climate warming as a function of forest cover extent and density to address the question of whether a more forested basin is more or less sensitive than a less forested basin to changes in climate. Currently, the DHSVM lacks the capability to incorporate forest growth and mortality in a dynamic manner. For all of these runs, we used the DHSVM set-up for the calibration period, in which we only changed the extent and fractional cover, keeping the remaining forest parameters constant, with climate forcing for the years 2001–2100.

Methods to analyse changes in streamflow patterns

Changes in streamflow patterns were evaluated using the COM (as in Stewart *et al*., 2005) and monthly

Table II. DHSVM vegetation scenarios for the A2 GFDL climate data

Vegetation cover	Scenario assumption
Current forest	Distributed forest (on 39% of the basin surface, extent shown in Figure 1), 80% fractional coverage over each forested pixel
All forest	Uniform forest cover, 80% fractional coverage over each pixel
Barren	Barren
Thinned	Distributed forest (on 39% of the basin surface, extent shown in Figure 1), 40% fractional coverage over each forested pixel

fractional flows (MFF), the ratio of flow volume in each month to the total flow volume of the water year. To test for existence of trends in the COM and MFF time series, we applied the Mann–Kendall test (Mann, 1945; Kendall, 1975; Helsel and Hirsch, 2002), a robust nonparametric test for trend, in which the null hypothesis assumed that COM and MFF are independent random variables (no trend). Prior to assigning the trend, we tested if the presence of autocorrelation in the time series was affecting the significance of the trend with algorithms provided in Yue *et al*. (2002). Because the Mann–Kendall test detects only the existence and direction of a trend, it was used in conjunction with Theil–Sen or Sen's slope estimator (Theil, 1950a, b, c; Sen, 1968), which quantified the magnitude of the linear trend (applied in Lettenmaier *et al*., 1994; Yue and Hashino, 2003). All trends are reported for 5% significance level.

To test whether the COM time series for the four vegetation scenarios are stochastically different (do not follow the same distribution), we used the nonparametric Mann–Whitney *U*-test (Mann and Whitney, 1947), also known as the Wilcoxon rank-sum test Wilcoxon (1945), for equality of the medians. The test has no underlying distribution of the data, and the null hypothesis assumes that any two COM series are drawn from the same distribution. The purpose of this test is to assess the uncertainty in the projected COM series for the four vegetation scenarios and to assign statistical confidence if the difference between scenarios is significant.

The changes in summer flows are important for meadow ecology and for estimating the water volumes that are to be distributed downstream for water supply. We used the Mann–Kendall trend tests to determine if trends exist in the lowest 7-day average low flows during the July to August period. Because the climate data are nonstationary, the typical probability distribution fitting technique to examine changes in frequency (e.g. Schnorbus and Alila, 2004; Kuraś *et al*., 2012) is not suitable, as the probability of occurrence of extreme events may change in time (Wigley, 2009). Instead, we used the simple discharge threshold technique (e.g. Tague *et al*., 2008) to illustrate the differences in frequency of occurrence of low flows between the model scenarios, in which for each scenario, a relative frequency is calculated as the number of years in which the lowest 7-day average low flow is less than a threshold value, divided by the total number of years.

RESULTS

Model evaluation for the historic period 2003–2009

The DHSVM performance for the 2003–2009 period was evaluated through comparing the modelled and observed hydrographs (Figure 3a, b) and SWE at the two snow pillow locations in the basin, Dana Meadows and Tuolumne Meadows, for the available record (Figure 3c,d). The Nash–Sutcliffe efficiency, *NSE* (Nash and Sutcliffe, 1970), and sum of the error squared (R^2) model evaluation criteria for the hydrograph (daily time step) were both equal to 0.87, indicating a good performance of the model to capture patterns of the observed hydrograph. Other classifications of *NSE* are more restrictive, such as that of James and Burges (1982) who suggest an *NSE* in excess of 0.95 as a very good performance. Errors are due to both model uncertainty and uncertainty in rating curve extrapolation at high flows. The model was able to represent the snow accumulation and melt for a range of climate conditions at the two snow pillow sites, Dana Meadows and Tuolumne Meadows, as shown in Figure 3c,d. The missing SWE observations in Figure 3c,d were due to instrument failure. A comprehensive discussion of the multiple factors affecting SWE observations beyond instrument failure is given in Johnson and Schaefer (2002).

Special consideration was given to representing the hydrograph recession limbs and the late summer low flows. Because summer precipitation is low (only 3% of the annual total during July to August period for 2003–2009), most of the summer flow results from high-elevation melt. Figure 3c,d shows that snow is disappearing at Dana Meadows (2966 m) around mid-June and at Tuolumne Meadows (2600 m) at the end of May, with an average difference of about 2 weeks. This difference is consistent with observations by Rice *et al*. (2011) that for elevations between 1800 and 3900 m, for each successively higher 300 m elevation band, snow disappeared 2–3 weeks later than the 300-m band below it.

Simulated changes in streamflow timing and magnitude as a function of vegetation cover in a warming climate

Temperature sensitivity tests. To explore the differences in hydrograph characteristics and SWE, as well as the changes in the energy balance components at forested and barren sites when temperature increases, we analysed the model output using the sensitivity tests described in the Climate Data and Model Scenarios Section. These tests were run for the calibration period 2003–2009, from which we extracted the 1 October 2003 to 1 October 2004 period (water year 2004) to illustrate the results. The 2003–2009 period included a range of conditions (Figure 3). Although water year 2004 was an average year, it was found representative for the types of changes seen in both wet and dry years. In the first set of tests (scenarios 1–4, Table I), in both temperature cases, historic T and historic $T + 3\,^{\circ}\mathrm{C}$, the forest COM occurred earlier than the barren COM, with decreased peak hydrographs (Figure 4a,c). In the case of the higher temperature, this difference was larger, increasing

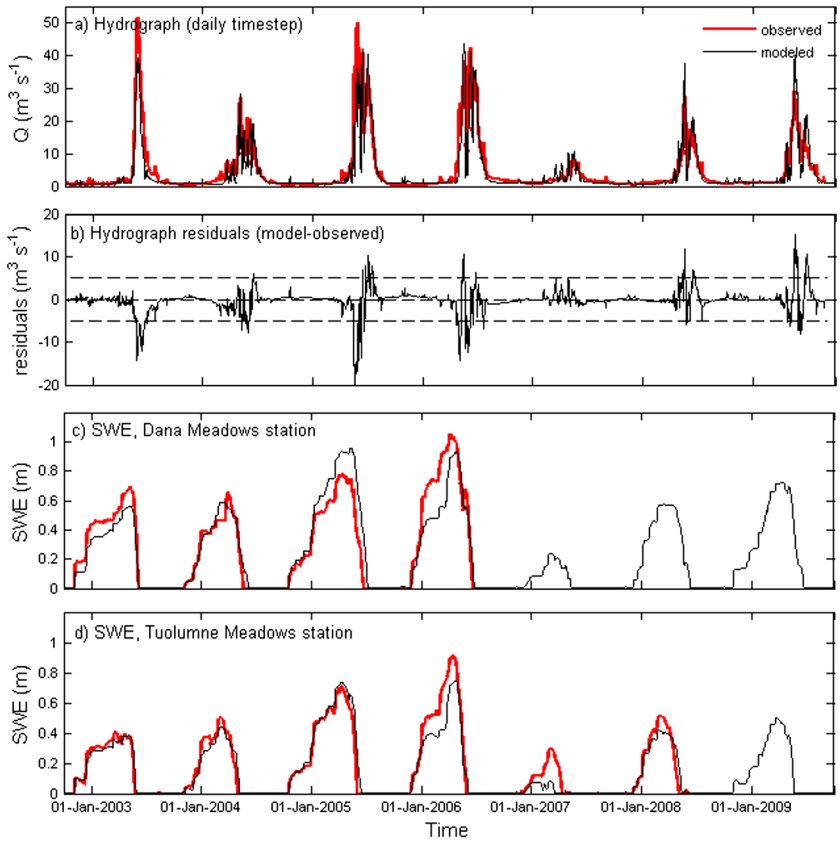

Figure 3. DHSVM calibration: a) simulated and observed daily hydrographs, b) hydrograph residuals, c) and d) simulated and observed SWE at Dana Meadows and Tuolumne Meadows sites, respectively. Horizontal dotted lines represent a visual reference level at 5 $m^3 s^{-1}$ for the hydrograph residuals

from 9 to 14 days. Winter temperatures exceeded 0 °C more frequently in the increased temperature scenario (Figure 4f, region C), generating snowmelt run-off (Figure 4a, region A). These midwinter peaks are more pronounced in the case of the forest (Figure 4a, region A) than in the case of barren (Figure 4c region B), because of increases in net longwave radiation, as further discussed in this section. Midwinter melt was not apparent in any of the historic *T* tests (Figure 4a,c).

The differences in streamflow timing depend on the snow accumulation and melt dynamics in the barren areas and under the forest. The simulated SWE at the flat Dana Meadows location (Figure 4b, d) shows that accumulation is higher when trees are not present because of the lack of canopy interception. Although snow accumulation on bare ground is similar in both temperature scenarios, during the melt period, the higher air temperature melts the snow earlier (Figure 4d), leading to earlier streamflow timing (Figure 4c). Higher air temperatures produced more winter melt than in the forest case (A in Figure 4a) than in the barren case (B in Figure 4c). The snow accumulation under the forest was therefore lower under warmer (+3 °C) temperatures than under historic temperatures (Figure 4b) because of winter melt events (Figure 4a,b). This thinner forest snowpack melted earlier than the barren snowpack in the increased temperature scenario (vertical line in Figure 4b,d). Forest evapotranspiration increased only 3% with temperature (Figure 4e); therefore, the changes in the forest hydrographs were mostly driven by the changes in snowmelt due to temperature increases.

Increases in temperature increase the energy balance components both in the barren areas and under the forest. Figure 5a–d shows the monthly energy balance components of the snowpack (estimated by summing the 3-hourly time series generated by the model described in Appendix A) for water year 2004 at Dana Meadows for the two vegetation scenarios. The absolute magnitudes of net shortwave and net longwave radiation were consistently larger for the barren scenario (Figure 5b,d) than the forest scenario (Figure 5a,c), but the net increases in the combined fluxes were larger for the forest case (Figure 5e) than the barren case (Figure 5f) for all months except May, June and July. Time series of turbulent fluxes, latent and sensible heat, were higher in the barren than in the forest case, but variations around zero caused monthly values to be small for all scenarios. For the forest case, the net longwave radiation increases most, followed by increases in latent heat flux and

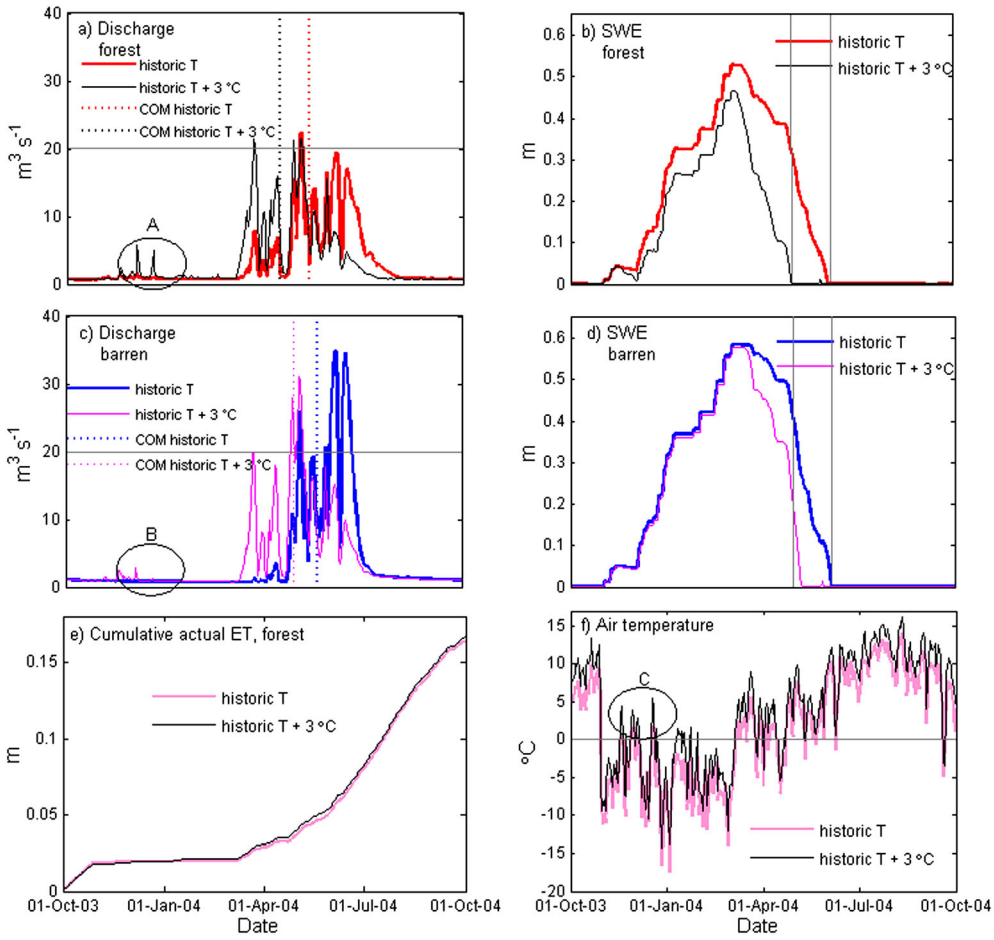

Figure 4. a) Simulated daily hydrographs assuming historic and increased air temperatures (+3 °C) for uniform forest scenario and for b) barren scenario; c) and d) SWE levels for the same scenarios at Dana Meadows, respectively; e) forest cumulative actual evapotranspiration; f) historic and increased air temperature daily time series. Vertical lines identify COM for each hydrograph. All plots are shown for water year 2004. Horizontal (a, c) and vertical (b, d) continuous lines are reference thresholds. Circled regions A and B are periods of midwinter melt

sensible heat flux, and in March and April, increases in net shortwave radiation (Figure 5e). The model simulated changes in shortwave radiation (Figure 5e,f) because the albedo algorithm is based on the simulated snow surface temperature (Equations (A6) and (A7), Appendix A), which was higher in the increased temperature scenario.

These changes are most evident in the spring and summer, although the smaller winter increases were enough to cause December and January melting in the +3 °C forest scenario when no melt occurred in those months during the base case run (Figures 4 and 6). Increases in energy balance components were larger in the forest case than the barren case in March, primarily because of greater increases in net longwave radiation (Figure 5e,f). Although the monthly melt rates were still higher in the barren case during March and April for both the base case and warmer scenarios (Figure 6), the combination of interception (a thinner initial snowpack, Figure 4b), midwinter melt (Figure 4a) and greater increases in melt rates in December, January and March (Figure 6b, c) led to the snowpack under the forest melting earlier than the snowpack on the bare ground in the +3 °C scenario.

Climate change scenario. The ΔT sensitivity tests helped identify the changes in the hydrograph and energy balance components when temperature alone is increasing. Using a long-term (2001–2100) climate change scenario in which both temperature and precipitation change in concert, we tested if the patterns were robust in a projected future scenario for the Tuolumne region. All DHSVM climate vegetation runs assumed the same future scenario derived from the GFDL global climate model A2 warming scenario, as previously described. The COM corresponding to the current vegetation scenario advanced by approximately 40 days, with an estimated Sen's slope of about 0.4 days year^{-1} (Figure 7a,b). The trends of earlier, simulated COM were found to be statistically significant for

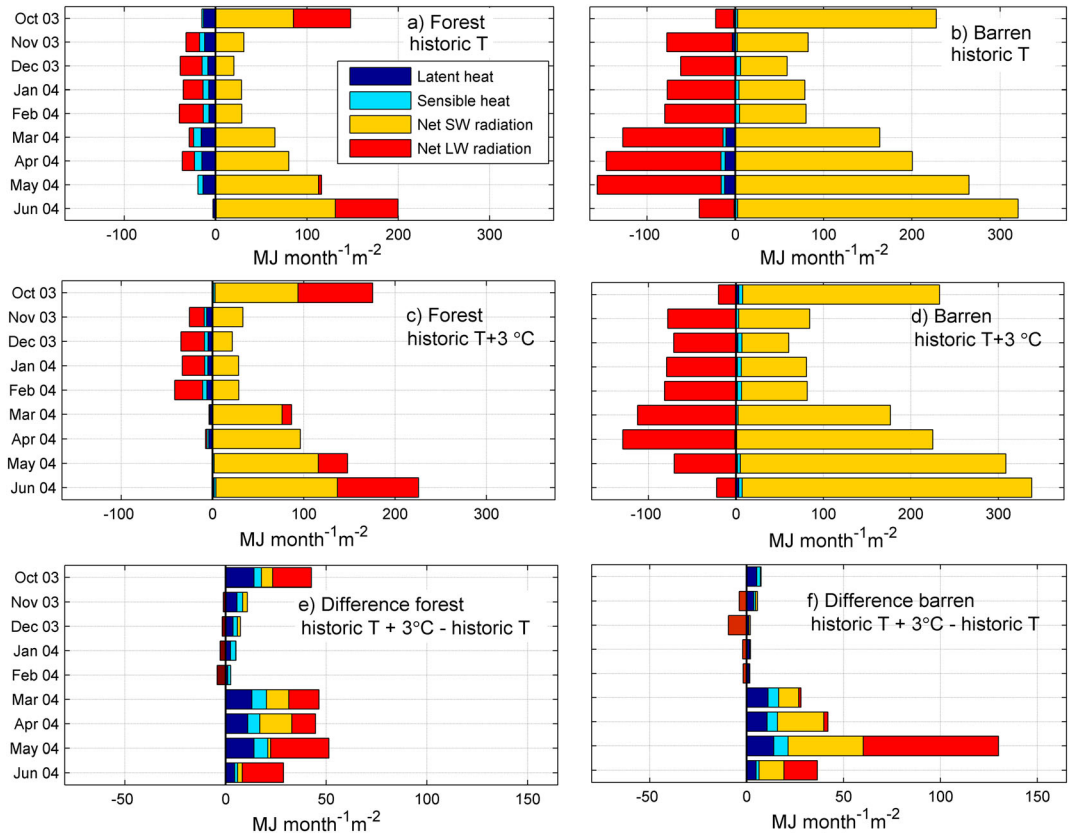

Figure 5. Monthly simulated energy balance components at Dana Meadows using historic temperature for a) forest coverage and for b) barren coverage; monthly energy balance components using a 3 °C increase in temperature for c) forest and for d) barren; monthly differences in energy balance components between the two temperature scenarios for e) forest and for f) barren. Note that the *x*-axis in e and *f* is different from a–d

all vegetation scenarios, using the Mann–Kendall tests at the 95% confidence level. COM advances exceeded 1 month in all vegetation scenarios (Figure 7a). Figure 7b shows Sen's slopes magnitudes representing the rates of COM displacement, which correspond from highest to lowest to all forest, current forest, thinned and barren, respectively.

Wilcoxon rank-sum tests on the COM vegetation time series indicated pairwise differences in the medians between the current forest, all forest and barren scenarios, respectively, showing that these COM series are stochastically different at a 95% confidence level (Figure 7c,d). However, no significant difference was found between the current forest and the thinned forest and between the barren and thinned forest scenarios, respectively (Figure 7c,d).

Vegetation cover affects not only timing but also the streamflow magnitude. This is illustrated in Figure 8a–d that shows the 20-year average monthly hydrographs during the 2001–2100 simulation period for the four vegetation scenarios. In the all forest scenario (Figure 8b), the hydrograph peak was smaller than in both the current vegetation (Figure 8a) and all barren (Figure 8c) scenarios, as there were increased losses to interception, sublimation and evapotranspiration. This effect is consistent with observations both from paired watershed and from modelling studies (e.g. Jones and Post, 2004; Schnorbus and Alila, 2004). Modelled differences in peak flows in DHSVM are mostly explained by the interception effects (e.g. Whitaker *et al.*, 2002).

The largest monthly flows of the year (May to July) were on average about 20% smaller in the all forest scenario (Figure 8b) compared with the base case current vegetation (Figure 8a) scenario, whereas barren (Figure 8c) and thinned (Figure 8d) forest flows were both on average higher (19% and 13%, respectively) than the base case vegetation scenario (Figure 8a), over all periods simulated. However, early spring (March to April) flows were consistently the largest in the all forest (Figure 8b) scenario, resulting in earlier COM timing. Late-winter and early spring flows (January to March) were higher by 30–40% in the all forest (Figure 8b) scenario and lower by about 24% over the same period in the all barren (Figure 8c) scenario compared with the current vegetation (Figure 8a) scenario. Peak summer flows decreased with increasing temperature over the 100-year simulation period by about 22%, 27%, 16% and 18% for the current forest, all forest, barren and

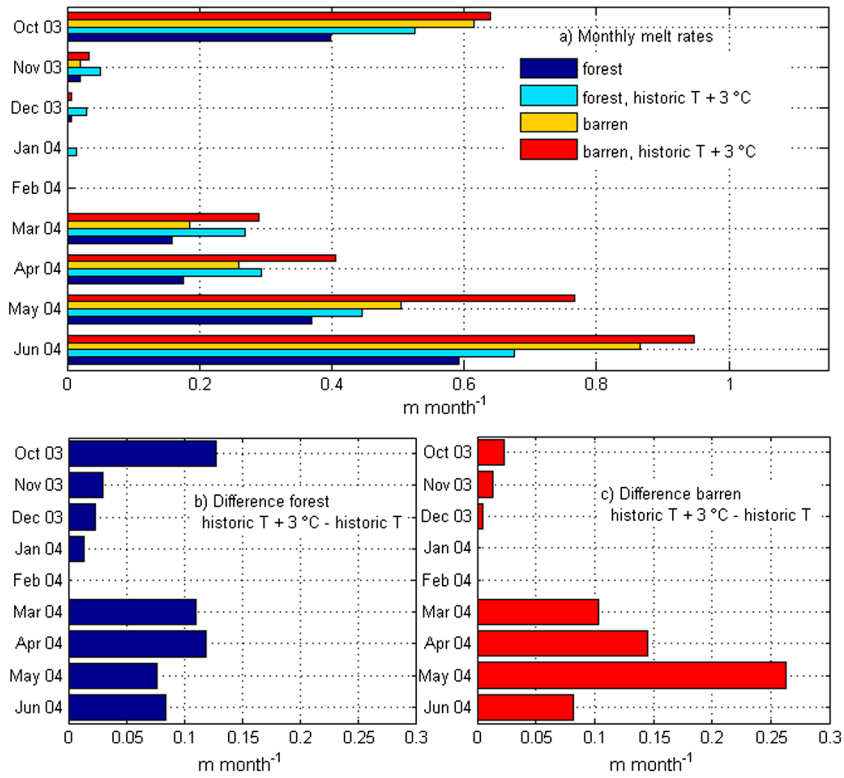

Figure 6. a) Monthly melt rates at Dana Meadows using historic and increased temperature for forest and for barren scenarios, b) difference in monthly melt rates using historic and increased temperature for forest, c) difference in monthly melt rates using historic and increased temperature for barren surface

thinned forest scenarios, respectively. These larger differences are also due to the lower precipitation during the last 20 years of the series (Figure 2b).

Changes in the hydrograph were determined by the trends in MFFs shown in Figure 8e along with the 95% confidence intervals for the slope. Trends are significant if the 95% confidence intervals do not intersect the zero line. The steepest trends for all vegetation scenarios were in May (increases in MFF) and July (decreases in MFF), whereas during the fall months (October, November and December), there were no significant trends. The winter to spring MFF trends (January through April) are significantly steeper in the all forest scenario than in the all barren scenario (Figure 8e). This effect is also illustrated by the ΔT sensitivity runs (Figure 4a,b), where the COM advanced at a higher rate in the all forest scenario, determining the steeper trends in winter MFFs shown in Figure 8e. Thus, when the forest is present, there is an increased tendency for midwinter melt than under barren conditions. This difference is driven by the trends in the energy balance components. For example, trend tests at the flat Dana Meadows location for forest and barren, the two extreme cases, showed that the temperature-dependent components such as the monthly latent heat, sensible heat and net radiation (for functional forms, see Appendix A) have positive trends for under the forest, compared with no trends or negative trends in the barren case during the January to April period.

The earlier snowmelt led to lower summer flows in all vegetation scenarios, with the most significant change occurring in July (Figure 8a–d). Thus, the Mann–Kendall tests showed significant declining trends over the 100-year period in the 7-day average lowest flows for the July to August period. Barren conditions were likely to provide the highest summer flows, followed by thinned, current forest and all forest conditions (Figure 9a,b). The all forest scenario had the highest frequency of 7-day low flows below $2.0\,m^3\,s^{-1}$, followed by current forest, thinned and barren (Figure 9c). The fixed threshold value used to calculate the relative frequencies was $2.0\,m^3\,s^{-1}$, the average summer (July to August) lowest flows in the current forest scenario for the entire climate model period (Figure 9a,b). Compared with this value, the same average lowest flows for barren and thinned are 23% and 9% higher, whereas for all forest, is 27% lower.

DISCUSSION

The most important changes in projected streamflow patterns for the current forest cover in the upper Tuolumne basin in the Sierra Nevada Mountains were shifts to earlier snowmelt due to increased temperature,

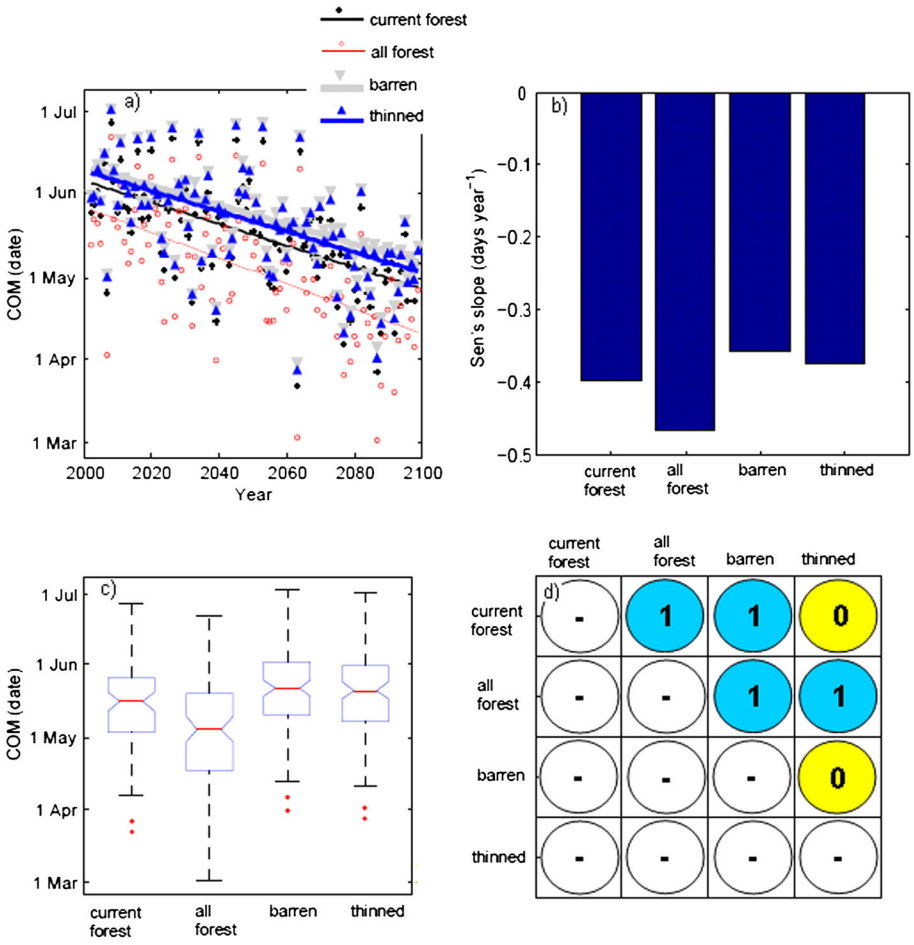

Figure 7. a) Centre of mass, COM, for the four vegetation scenarios, b) Sen's slope of COM change, c) boxplots of the COM series, and d) diagram showing results from the Wilcoxon rank-sum test for the medians between combinations of any two COM series of the four vegetation scenarios: 0 indicates that the null hypothesis that the two COM series are drawn from the same distribution cannot be rejected at the 95% confidence level, and 1 indicates a rejection of the null hypothesis

with higher winter flows and reduced peak and late summer flows. Similar hydrologic changes in response to climate warming were found at a lower elevation in the Tuolumne basin based on hydrologic simulations encompassing a much larger drainage area (3970 km^2), stretching over 1600 m elevation range (Maurer, 2007). The idealized modelling experiments explored in this study showed that forest plays an important role in the rate of streamflow advances to earlier dates in response to climate warming. Thus, a less vegetated basin was able to maintain a thicker and colder snowpack that melted later in the season.

Under barren conditions, the modelled accumulation was higher by about 10–30%, than under the forest, mostly as a result of the lack of canopy interception. This range is consistent with field measurements in lodgepole pine (*P. contorta*) stands that have shown that snow accumulation in the barren areas can be 10–40% higher than under the forest and as high as 80–85% in some locations (summary from Table II in Murray and Buttle, 2003). With increasing temperature, the modelled difference in accumulation tended to widen with temperature as a result of increasing midwinter melt, and it was more pronounced at lower elevations (Figure A1b,d,f,h).

Modelled melt rates were higher in the barren areas than under the forest during the spring–summer melting period (Figure 6), but the thinner snowpack under the trees melted earlier, especially at lower elevations (Figures 4b,d and A1b,d,f,h). In a different modelling experiment, Strasser *et al.* (2011) showed that snow disappearing earlier under the forest or in the barren areas may depend on the snowpack thickness. At the flat Dana Meadows and Tuolumne Meadows locations, modelled snow disappeared earlier under forested conditions during average years (e.g. 2004, Figures 4b,d and A1b,d,f,h) and also during dry and wet years of the 2003–2009 period (figures not shown). This under the forest melting pattern was robust despite uncertain forest parameterization, as

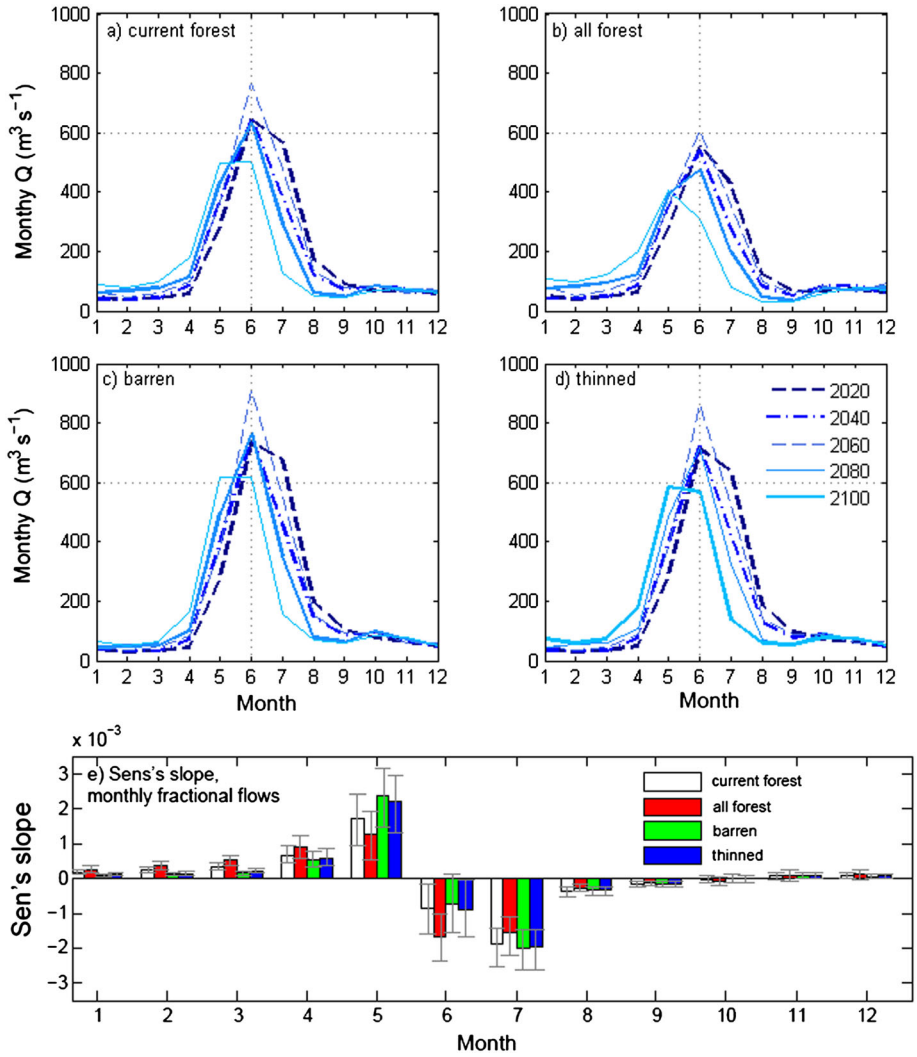

Figure 8. a) Twenty-year average monthly hydrographs for current forest, b) all forest, c) barren and d) thinned forest scenarios, respectively; e) Sen's slope for monthly fractional flows for the entire 2001–2100 simulation period

shown in Appendix A, Figure A1b,d,f,h. Midwinter melt (both rate and volume) was higher when the snowpack under the forest was thinner. Figure 6b,c shows that in contrast to the warm period (May and July), during the cold period (October and January) under the influence of higher winter temperatures, melt rates have a more significant increase under the forest. Midwinter melt was most evident during December and January, when for historic temperatures, there was little to no melt in both forested and barren cases, but when temperatures were increased above 0 °C values for several days, melt occurred under the forest (Figure 6a).

Slope, aspect, wind and elevation all play important roles in the snow accumulation and melt patterns. For example, on the south-facing slopes, the snow melted faster in the barren areas than under the forest, whereas on the north-facing slopes, the snow melted faster under the forest in an eastern Canadian Rocky Mountain basin (Ellis *et al.*, 2011). The upper Tuolumne basin has both north-facing and south-facing slopes, but the north-facing slopes are predominant. Most of the currently nonforested regions are north facing, topographically shaded (Figure 1). Our simulations showed that the overall effect of the increase in the net longwave radiation with increases in air temperature was to melt the snow under the forest faster. The increased midwinter melt under warming temperatures illustrated in Figures 4a,b and 6 determined earlier snow disappearance dates at forested sites (Figure 4b) than at barren sites (Figure 4d) at flat locations. Because of the additional snow depth variability with local topography and wind, these snowmelt patterns may not occur similarly at all sites. However, the overall response of the basin was to provide higher and later peak spring flows and higher late summer flows when assuming reduced forest coverage. The

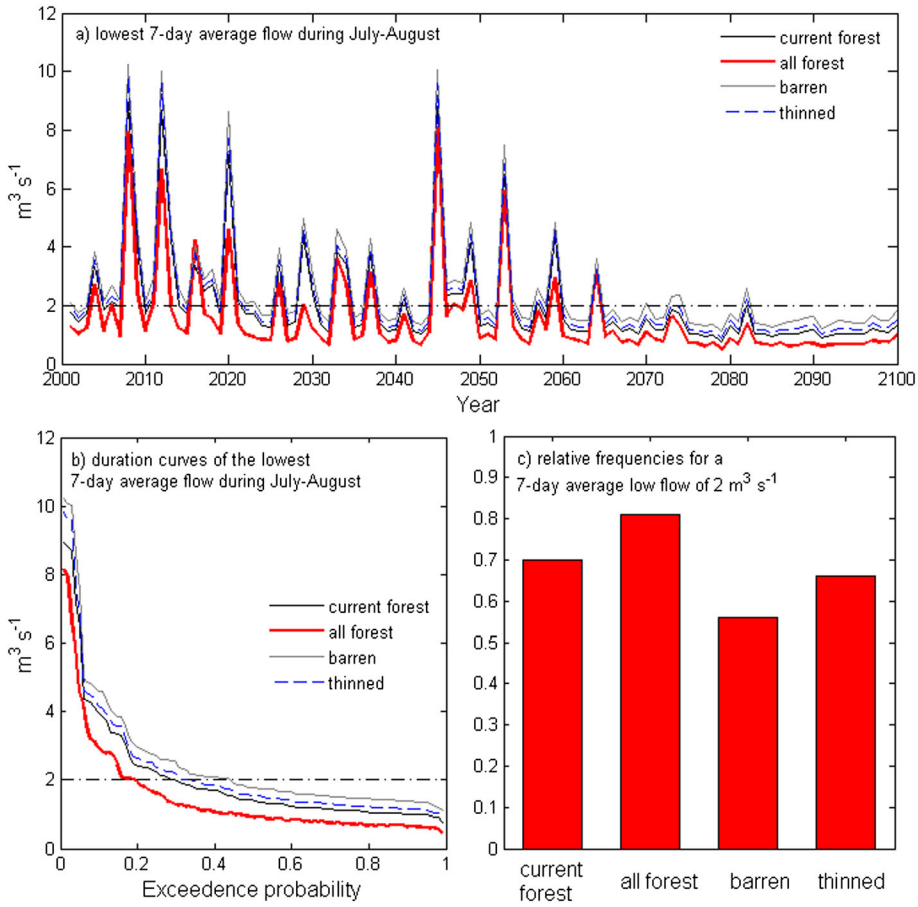

Figure 9. a) Lowest 7-day average low flow during July to August each year for the four vegetation scenarios, b) duration curves for the July to August 7-day average lowest flows, and c) relative frequencies, as the number of years in each the lowest 7-day average was below a threshold value (2 $m^3 s^{-1}$) divided by the total number of years

role of wind distribution likely would increase with the removal of all forest cover. One hydrologic effect could be an increase in the heteorogeneity of snow accumulation, which would lead to longer-lasting late-season streamflow as noted in Reynold's Creek by Luce *et al.* (1998). This effect would thus also support our conclusion of more late-summer streamflow under reduced forest cover, but precise quantification of the role of wind redistribution is beyond the scope of our current study.

Field studies also reported that melt rates during the spring were generally higher in the barren regions or in clear-cut areas than under the forest (Murray and Buttle, 2003; Boon, 2009; Burles and Boon, 2011; Winkler, 2011), but the date of snow disappearance was found to vary as a function of location, aspect, snowpack thickness and canopy density. For example, snow cover loss occurred earlier by several days in a damaged forest or a clear-cut than in a mature forest in the interior of British Columbia, Canada (Boon, 2009; Burles and Boon, 2011; Winkler, 2011), whereas in central Ontario, for the same slope aspect, the snow disappeared simultaneously in the barren areas and under the forest (Murray and Buttle, 2003). These sites were located in a colder climate than the Tuolumne site, with lower chances of midwinter melt events.

Although there is significant spatial variability, as discussed earlier, reported field measurements in the Sierra Nevada Mountains indicate that snow in this region generally disappeared earlier or at about the same time under the forest than in the barren areas (Kittredge, 1953; Lundquist and Lott, 2008; Bales *et al.*, 2011a; Kerkez *et al.*, 2012). Early historical observations from the 1930s and 1940s in the Central Sierra showed that snow disappeared earlier in regions with lower percentages of canopy cover (figure shown on p. 54, Kittredge, 1953). Spring (after March 9) melt rates were higher in the open than under the forest, but winter (before March 9) melt rates were higher under the forest for several years and most forest types (Table 28, Kittredge, 1953). DHSVM SWE simulations in the Tuolumne area showed that at the two snow pillow locations, the snow cover loss occurred earlier under the forest than in the barren areas (Figures 4b,d

and A1b,d,f,h). This effect is more pronounced with increasing temperatures and midwinter melt events. Recent areal imagery taken in mid-June of 2011 north of the Tuolumne area (38°48′56″, 120°06′35″) exemplifies these findings (Figure A2). This image shows the snow disappearing first around the trunks of the trees, where melt rates have been found to be higher (Pomeroy *et al.*, 2009; Veatch *et al.*, 2009). Additional observational evidence of where and analysis of why snow lasts longer under forest cover versus in the barren areas remains a topic for future investigation.

The dynamics of snowmelt change with increasing temperature in both barren and forested scenarios. Field and modelling studies have found that incoming shortwave radiation and turbulent fluxes were higher in the barren regions than under the forest (Hardy *et al.*, 1997; Link and Marks, 1999a, b; Sicart *et al.*, 2004; Boon, 2009). Ablation in the barren areas is controlled by the shortwave radiation, whereas net longwave radiation has a smaller contribution to melting (Boon, 2009). In contrast, under the forest, longwave radiation has a higher contribution to melting (Boon, 2009; Burles and Boon, 2011). In the Tuolumne area, model temperature sensitivity tests showed that increases in temperature determined increases in both the net longwave radiation and turbulent fluxes under the forest that are higher than the increases in the barren areas. These changes triggered higher melt rates under the forest, causing even earlier snow disappearance dates and exacerbating the effects of climate change in terms of streamflow timing advancing towards earlier dates. Temperature increases had a modest effect (3%) on simulated forest evapotranspiration in this area. This effect is similar to findings of Safeeq and Fares (2011) who reported small increases of modelled DHSVM evapotranspiration with temperature alone (0.5% and 2% for a temperature increase of 1.1 and 6.4 °C).

Uncertainties in our upper Tuolumne simulations fall into three general categories, related to (i) the trend of future carbon emissions, (ii) the climate model output and downscaling procedures and (iii) the hydrologic model. Current observations suggest that the A2 emissions scenario may be a conservative estimate of temperature change given current global trends in CO_2 (Manning *et al.*, 2010) and that the large-scale temperature increases may be even larger than those considered in this study. There is recognized uncertainty about the GCMs' ability to predict changes in large-scale weather patterns, particularly as they relate to precipitation (e.g. Dai, 2006; Maraun *et al.*, 2010). This uncertainty from the GCMs may be larger than the uncertainty from the hydrologic models (Teng *et al.*, 2012), which primarily stems from the hydrologic model structure and model parameterization. In the Tuolumne area, the model tests showed that even when considering a relatively large uncertainty in forest parameterization, the model simulated snow disappearing faster under the forest than in the barren regions, with this effect enhanced at higher temperatures. We have only investigated these changes with one model, which has structural model uncertainty (see discussion in Clark *et al.*, 2008) and for one climate model and for one basin. The most important finding of this study is that combined forest-change and temperature-change effects on streamflow are not linear and are not negligible and therefore should be considered in future research. This is a complicated topic that will require multiple models, multiple forest types and multiple watersheds across different climate regions to fully address. Therefore, a full evaluation of the uncertainty associated with our modelled scenarios is beyond the scope of this study.

Management decisions in snowmelt-dominated areas such as Tuolumne Meadows, which are dependent on streamflow timing and magnitude for ecological purposes, can expect differing sensitivities to vegetation cover in a warming climate. The upper Tuolumne area is in Yosemite National Park, where timber is not harvested. However, results from the virtual experiments evaluated in this study can be useful to other regional basins where forest management actions are considered for summer flow augmentation. For example, Bales *et al.* (2011b) investigated forest management actions that can increase summer water yield on the west-side of the Sierra Nevada at 1500–3600 m elevation and suggested that canopy reduction through forest thinning has the potential to improve snow retention and increase streamflows. Preliminary results indicated that a reduction in forest cover by about 40% could increase the water yield by about 9% (Bales *et al.*, 2011b). These estimations are in agreement with the results from this study and the earlier findings of Kittredge (1953). Model simulations performed in the upper Tuolumne for the thinned forest scenario, in which the canopy cover is reduced to 50% of the current levels, showed similar ranges: increases in the peak and late summer flows by about 13% and 9%, respectively.

The results presented here emphasize the importance of understanding the combined effects of temperature and vegetation on snowmelt and streamflows. These complex relationships depend on the geographic location, elevation and site conditions. Although in general more snow accumulates in the gaps than under the forest (see also reviews in Ellis *et al.*, 2013; Varhola *et al.*, 2010), the melt dynamics may differ between open and forest areas such that the date of the year where the snow first disappears, in the open or under the forest, varies as function of climate and local topography (Ellis *et al.*, 2013). In the high elevations of the Sierra Nevada, snow generally persists longer in the open than under the forest

in many areas also because the region's precipitation falls primarily as snow during the winter, leaving little opportunity for the spring snowfall to compensate for the midwinter melt caused by increasing temperatures. The overall effects of elevation, topography and precipitation patterns on the variable snow disappearance dates as a function of forest density in the Sierra Nevada are very well illustrated by the data collection of Kittredge (1953).

Using modelling experiments, Strasser *et al*. (2011) also showed that snowmelt in the open areas and under the forest depends on snowfall patterns. They indicated that midwinter melt can occur under the forest when little snow was available to melt, with snow persisting longer in the open areas than under the forest, especially on north-facing slopes. When more snow was available on the ground, snow disappeared earlier in the open areas. Differences in snow persistence duration between the forested and open areas were largest for the south-facing slopes. These variable effects were mediated by the variable contribution of the shortwave and longwave radiation to melting as a function of slope, time of the year and snow depth. In this study, we showed that in the early winter months, forest snowmelt may occur because of increased contribution of longwave radiation. Because of its dependence on temperature, longwave radiation is expected to play an increasing role in snowmelt dynamics under the forest, as temperatures warm.

Given the large variability in snowmelt at the hillslope scale, the overall effects of different forest covers on streamflows can be evaluated at the basin scale through distributed hydrologic modelling. Here, we exemplified the use of such a model for evaluating the role of vegetation cover on streamflow timing and magnitude in the context of climate change for the case study of the upper Tuolumne basin in the Sierra Nevada Mountains. In this system, less vegetation increases snow retention, leading to increases in spring and summer flows, which could improve downstream water supplies and meadow ecosystems. Although forest is not harvested in this area, controlled burned or insect-infested forest areas may increase snow retention in the future. In addition to flow augmentation, thinner forests may also reduce fire risks, which are becoming higher with increasing temperatures (Graham *et al*., 2004). Thus, the interactions presented here are key issues to consider in managing the entire integrated mountain ecosystem.

SUMMARY AND CONCLUSIONS

The amount of snowmelt water in the streams and the streamflow timing are important for the montane ecosystems and for downstream water supply. In this study, we investigated, through hydrologic model simulations, the role of the vegetation cover in the rate of changes in streamflow patterns in the upper Tuolumne River basin in the Sierra Nevada Mountains when temperatures rise. We employed four different vegetation scenarios: current forest, forest on the entire basin, barren and thinned forest for a 3.9 °C warming scenario. We also used sensitivity tests to evaluate changes in modelled energy balance components as a result of increasing temperatures and to assess the uncertainty in model forest parameterization.

We found that in the current forest cover scenario, warming temperatures caused earlier snowmelt timing, with increased midwinter melt and decreased peak and late summer flows. These effects were greater when forest was assumed to cover the entire basin area. Thus, the COM, the date on which fractional cumulative discharge reaches 50%, occurred earlier in the season by about 12 days on average, and the rate of its advancing was higher by about $0.06\,\text{days}\,\text{year}^{-1}$ than for the current forest scenario over the 100-year period, with increased volume of midwinter melt and lower peak and late summer flows.

In contrast, a less vegetated basin maintains a thicker snowpack that disappears later in the season, increasing peak and late summer flows and delaying streamflow timing. Modelled accumulation was lower under the forest than in the barren areas because of interception and midwinter melt. Melt rates were higher in the barren regions than under the forest, but the thinner snowpack under the forest disappeared earlier. Both melt rates in the barren areas and under the forest increase with increasing temperatures. The magnitudes of these effects depend on the slope orientation. Maximizing snowpack retention has the potential to decrease the rate of streamflow timing advancing to earlier dates and to increase summer flows.

Temperature-controlled energy balance components (longwave radiation and turbulent fluxes) increased more under the forest than in the barren regions in a warming climate. These changes increase melt rates and midwinter melt. Longwave radiation has a higher fractional contribution to melting in early spring when shortwave radiation is lower. In a warmer climate, the forests melted the snow faster because of increases in net longwave radiation that are more significant at temperatures higher than 0 °C.

Understanding forest hydrologic processes in the context of climate change is important for identifying system sensitivity as a function of forest cover when temperatures rise. Using the upper Tuolumne basin as a case study, we found that there is a combined effect of both temperature and vegetation on streamflows. In the Tuoulmne area, less canopy cover increased snow retention, delayed streamflow timing and increased peak and late summer flows. Both observational and modelling studies in other regions of the world are needed to provide additional insights about the snow–vegetation interactions in other climatic conditions,

topographies and vegetation cover, and with different model structures and conceptualizations.

ACKNOWLEDGMENTS

We thank Jim Roche, Brian Huggett and Heidi Roop for their help with field data collection and Fred Lott and Jeff Deems for the initial set-up of DHSVM. We thank Nick Burmeister for his help with multiple computer issues and transfers and Steve Burges and Alan Hamlet for their initial review of the manuscript. This research was supported by the National Science Foundation under grant no. CBET-0729830, grant no. CBET-0729838, and grant no. CBET-0931780.

REFERENCES

Alila Y, Beckers J. 2001. Using numerical modelling to address hydrologic forest management issues in British Columbia. *Hydrological Processes* **15**: 3371–3387.

Alila Y, Kuraś PK, Schnorbus M, Hudson R. 2009. Forests and floods: a new paradigm sheds light on age-old controversies. *Water Resources Research* **45**, doi:10.1029/2008WR007207.

Andreadis KM, Storck P, Lettenmaier DP. 2009. Modeling snow accumulation and ablation processes in forested environments. *Water Resources Research* **45**, doi:10.1029/2008WR007042.

Andreassian V. 2004. Waters and forests: from historical controversy to scientific debate. *Journal of Hydrology* **291**: 1–27.

Bales RC, Hopmans J, O'Geen T, Meadows M, Hartsough PC, Kirchner P, Hunsaker CT, Beaudette D. 2011a. Soil moisture response to snowmelt and rainfall a Sierra Nevada mixed-conifer forest. *Vadose Zone Journal* **10**(3): 786–799.

Bales RC, Battles JJ, Chen Y, Conklin MH, Holst E, O'Hara KL, Saksa P, Stewart W. 2011b. Forests and water in the Sierra Nevada: Sierra Nevada Watershed Ecosystem Enhancement Project. Sierra Nevada Research Institute report number 11.1.

Battin J, Wiley MW, Ruckelshaus MH, Palmer RN, Korb E, Bartz KK, Imaki H. 2007. Projected impacts of climate change on salmon habitat restoration. *Proceedings of the National Academy of Sciences* **104**(16): 6720–5.

Beckers J, Smerdon B, Wilson M. 2009. Review of hydrologic models for forest management and climate change applications in British Columbia and Alberta. FORREX Forum for Research and Extension in Natural Resources, Kamloops, BC FORREX Series 25; 166. http://www.forrex.org/sites/default/files/forrex_series/FS25.pdf

Bewley D, Alila Y, Varhola A. 2010. Variability of snow water equivalent and snow energetics across a large catchment subject to Mountain Pine Beetle infestation and rapid salvage logging. *Journal of Hydrology* **388**: 464–479.

Boon S. 2009. Snow ablation energy balance in a dead forest stand. *Hydrological Processes* **23**: 2600–2610.

Bristow RL, Campbell GS. 1984. On the relationship between incoming solar radiation and daily maximum and minimum temperature. *Agricultural and Forest Meteorology* **31**: 159–166.

Burles K, Boon S. 2011. Snowmelt energy balance in a burned forest plot, Crowsnest Pass, Alberta. Canada. *Hydrological Processes* **25**: 3012–3029, doi:10.1002/hyp.8067.

Carsel RF, Parrish RS. 1988. Developing joint probability distributions of soil water retention characteristics. *Water Resources Research* **24**: 755–769, doi: 10.1029/WR024i005p00755.

Cayan DE, Maurer EP, Dettinger MD, Tyree M, Hayhoe K. 2008. Climate change scenarios for the California region. *Climatic Change* **87**: 21–42.

Clark MP, Slater AG, Rupp DE, Woods RA, Vrugt JA, Gupta HV, Wagener T, Hay LE. 2008. Framework for Understanding Structural Errors (FUSE): a modular framework to diagnose differences between hydrological models. *Water Resources Research* **44**, *W00B02*, doi:10.1029/2007WR006735.

Cuo L, Lettenmaier DP, Alberti M, Richey JE. 2009. Effects of a century of land cover and climate change on the hydrology of the Puget Sound basin. *Hydrological Processes* **23**(6): 907–933.

Cuo L, Beyene TK, Voisin N, Su FG, Lettenmaier DP, Alberti M, Richey JE. 2011. Effects of mid-twenty-first century climate and land cover change on the hydrology of the Puget Sound basin, Washington. *Hydrological Processes* **25**(11): 1729–1753.

Dai A. 2006. Precipitation characteristics in eighteen coupled climate models. *Journal of Climate* **19**: 4605–4630.

Daly C, Neilson P, Phillips DL. 1994. A statistical-topographic model for mapping climatological precipitation over mountainous terrain. *Journal of Applied Meteorology* **33**: 140–158.

Daly C, Gibson WP, Taylor GH, Johnson GL, Pasteris P. 2002. A knowledge-based approach to the statistical mapping of climate. *Climate Research* **22**: 99–113.

Daly C, Halbleib M, Smith JI, Gibson WP, Doggett MK, Taylor GH, Curtis J, Pasteris PP. 2008. Physiographically sensitive mapping of climatological temperature and precipitation across the conterminous United States. *International Journal of Climatology* **28**: 2031–2064 DOI: 10.1002/joc.1688.

Delworth T, Broccoli AJ, Rosati A, Stouffer RJ, Balaji V, Beesley JA, Cooke WF, Dixon KW, Dunne J, Dunne KA, Durachta JW, Findell KL, Ginoux P, Gnanadesikan A, Gordon CT, Griffies SM, Gudgel R, Harrison MJ, Held IM, Hemler RS, Horowitz LW, Klein SA, Knutson TR, Kushner PJ, Langenhorst AR, Lee H-C, Lin S-J, Lu J, Malyshev SL, Milly PCD, Ramaswamy V, Russell J, Schwarzkopf MD, Shevliakova E, Sirutis JJ, Spelman MJ, Stern WF, Winton M, Wittenberg AT, Wyman B, Zeng F, Zhang R. 2006. GFDL's CM2 global coupled climate models – Part 1: formulation and simulation characteristics. *Journal of Climate* **19**: 643–674.

Ellis CR, Pomeroy JW, Essery RLH, Link TE. 2011. Effects of needleleaf forest cover on radiation and snowmelt dynamics in the Canadian Rocky Mountains. *Canadian Journal of Forest Research* **41**: 608–620.

Ellis CR, Pomeroy JW, Link TE. 2013. *Modeling increases in snowmelt yield and desynchronization resulting from forest gap-thinning treatments in a northern mountain headwater basin*. Water Resour. Res. **49**, doi:10.1002/wrcr.20089.

Epke G, Finger M, Lusardi R, Marks N, Mount J, Nichols A, Null S, O'Rear T, Purdy S, Senter, A, Viers J. 2010. Confluence: a natural and human history of the Toulumne River watershed. Department of Geology and Center for Watershed Sciences, University of California Davis Mount J, Purdy S (Eds); 189. http://watershed.ucdavis.edu/tuolumne/resources/ConfluenceTuolumneV1.pdf , last accessed August 6, 2012.

Graham RT, McCaffrey S, Jain TB. 2004. Science basis for changing forest structure to modify wildfire behavior and severity, General Technical Report RMRS-GTR-120. U.S. Department of Agriculture, Forest Service, Rocky Mountain Research Station: Fort Collins; 43.

Grant GE, Lewis SL, Swanson FJ, Cissel JH, McDonnell JJ. 2008. Effects of forest practices on peak flows and consequent channel response: a state-of-science report for western Oregon and Washington, General Technical Report PNW-GTR-760, Pacific Northwest Research Station United States Department of Agriculture, Portland, Oregon.

Hamlet AF, Lettenmaier DP. 1999. Effects of climate change on hydrology and water resources in the Columbia River basin. *American Water Resources Association* **35**(6): 1597–1623.

Hardy JP, Davis RE, Jordan R, Li X, Woodcock C, Ni W, McKenzie JC. 1997. Snow ablation modeling at the stand scale in a boreal jack pine forest. *Journal of Geophysical Research* **102**(D24): 29,397–29,405.

Hardy JP, Melloh R, Koenig G, Marks D, Winstral A, Pomeroy J, Link T. 2004. Solar radiation transmission through conifer canopies. *Agriculture and Forest Meteorology* **126**: 257–270.

Helsel DR, Hirsch RM. 2002. Statistical methods in water resources: U.S. Geological Survey Techniques of Water-Resources Investigations, book 4, chap. A3; 524.

Hewlett JD. 1971. Comments on the catchment experiment to determine vegetal effects on water yield. *Water Resources Bulletin* **7**(2): 376–381.

Hewlett JD. 1982. Principles of Forest Hydrology. The University of Georgia Press: Athens; 183.

Hidalgo H, Dettinger M, Cayan D. 2008. Downscaling with constructed analogues—daily precipitation and temperature fields over the United States: California Energy Commission PIER Final Project Report CEC-500-2007-123; 48.

Huber NK. 1987. The geologic story of Yosemite National Park. United States Geological Survey Bulletin, 1595; 64.

Idso SB. 1981. A set of equations for full spectrum and 8- to 14-μm and 10.5- to 12.5-μm thermal radiation from cloudless skies. *Water Resources Research* **17**: 295–304.

IPCC, Intergovernmental Panel on Climate Change. 2001. Special report on emissions scenarios, Chapter 4: An Overview of Scenarios / 4.2. SRES Scenario Taxonomy / Table 4–2: Overview of SRES scenario quantifications. (Available at: http://www.grida.no/publications/other/ipcc_sr/?src=/climate/ipcc/emission/091.htm#4.2.1.)

James LD, Burges SJ. 1982. Selection, calibration, and testing of hydrologic models. In *Hydrologic Modeling of Small Watersheds*, Haan CT, Johnson HP, Brakensiek DL (eds). American Society of Agricultural Engineers: St.Joseph, Mich.; 437–472.

Johnson JB, Schaefer G. 2002. The influence of thermal, hydrologic, and snow deformation mechanisms on snow water equivalent pressure sensor accuracy. *Hydrological Processes* **16**: 3529–3543, doi:10.1002/hyp.1236.

Jones JA, Post DA. 2004. Seasonal and successional streamflow response to forest cutting and regrowth in the northwest and eastern United States. *Water Resources Research* **40**, doi:10.1029/2003WR002952.

Jost GR, Moore D, Weiler M, Gluns DR, Alila Y. 2009. Use of distributed snow measurements to test and improve a snowmelt model for predicting the effect of forest clear-cutting. *Journal of Hydrology* **376**: 94–106.

Kendall MG. 1975. *Rank Correlation Methods*. Griffin: London; 196.

Kerkez B, Glaser SD, Bales RC, Meadows MW. 2012. Design and performance of a wireless sensor network for catchment-scale snow and soil moisture measurements. *Water Resources Research* **48**, W09515, doi:10.1029/2011WR011214.

Kittredge J. 1953. Influence of forests on snow in the ponderosa-sugar pine-fir zone of the central Sierra Nevada. *Hilgardia* **22**: 1–96.

Knutson TR, Delworth TL, Dixon KW, Held IM, Lu J, Ramaswamy V, Schwarzkopf MD, Stenchikov G, Stouffer RJ. 2006. Assessment of twentieth century regional surface temperature trends using the GFDL CM2 coupled models. *Journal of Climate* **10**: 1624–1651.

Kuraś PK, Alila Y, Weiler M. 2012. Forest harvesting effects on the magnitude and frequency of peak flows can increase with return period. *Water Resources Research* **48** doi: 10.1029/2011WR010705.

Kuraś PK, Alila Y, Weiler M, Spittlehouse D, Winkler R. 2011. Internal catchment process simulation in a snow-dominated basin: performance evaluation with spatiotemporally variable runoff generation and groundwater dynamics. *Hydrological Processes* **25**: 3187–3203, DOI:10.1002/hyp.8037.

Lettenmaier DP, Wood EF, Wallis JR. 1994. Hydro-climatological trends in the continental United States, 1948–88. *Journal of Climate* **7**: 586–607.

Leung LR, Wigmosta MS. 1999. Potential climate change impacts on mountain watersheds in the Pacific Northwest. *Journal of the American Water Resources Association* **35**: 1463–1471.

Leung LR, Qian Y, Bian X, Washington WM, Han J, Roads JO. 2004. Mid-century ensemble regional climate change scenarios for the western United States. *Climatic Change* **62**(1–3): 75–113.

Link T, Marks D. 1999a. Distributed simulation of snowcover mass and energy balance in a boreal forest. *Hydrological Processes* **13**: 2439–2452.

Link T, Marks D. 1999b. Point simulation of seasonal snowcover dynamics beneath boreal forest canopies. *Journal of Geophysical Research* **104**: 27 841–27 858.

Link T, Marks D, Hardy J. 2004. A deterministic method to characterize sub-canopy radiation environments. *Hydrological Processes* **18**(18): 3583–3594.

Liston GE, Elder K. 2006. A distributed snow-evolution modeling system (SnowModel). *Journal of Hydrometeor* **7**: 1259–1276. doi: http://dx.doi.org/10.1175/JHM548.1

Loheide SP II, Lundquist JD. 2009. Snowmelt-induced diel fluxes through the hyporheic zone. *Water Resources Research* **45** doi:10.1029/2008WR007329.

Loheide SPII, Deitchman RS, Cooper DJ, Wolf EC, Hammersmark CT, Lundquist JD. 2009. Hydroecology of impacted wet meadows in the Sierra Nevada and Cascade Ranges, CA. *Hydrogeology Journal* **17**: 229–246, doi: 10.1007/s10040-008-0380-4.

Lopez-Moreno JI, Latron J. 2008. Influence of forest canopy on snow distribution in a temperate mountain range. *Hydrological Processes* **22**(1): 117–126.

Lowry C, Deems J, Loheide SP II, Lundquist JD. 2010. Linking snowmelt derived recharge and groundwater flow in a high elevation meadow system, Sierra Nevada Mountains, California. *Hydrological Processes* **24**: 2821–2833.

Lowry C, Loheide SP II, Moore C, Lundquist JD, 2011. Groundwater controls on vegetation composition and patterning in mountain meadows. *Water Resources Research* **47** W00J11, doi:10.1029/2010WR010086.

Luce CH, Tarboton DG, Cooley KR. 1998. The influence of the spatial distribution of snow on basin-averaged snowmelt. *Hydrological Processes* **12**: 1671–1683.

Lundquist JD, Cayan DR. 2007. Surface temperature patterns in complex terrain: daily variations and long-term change in the central Sierra Nevada, California. *Journal of Geophysical Research* **112**, D11124, doi:10.1029/2006JD007561.

Lundquist JD, Lott F. 2008. Using inexpensive temperature sensors to monitor the duration and heterogeneity of snow-covered areas in complex terrain. *Water Resources Research*, special issue on Measurement Methods **44**, W00D16, doi:10.1029/2008WR007035.

Lundquist JD, Cayan DR, Dettinger MD. 2003. Meteorology and hydrology in Yosemite National Park: a sensor network application. In Information Processing in Sensor Networks, F. Zhao and L. Guibas (eds.): IPSN 2003, LNCS 2634, 518–528.

Lundquist JD, Cayan D, Dettinger M. 2004. Spring onset in the Sierra Nevada: when is snowmelt independent of elevation? *Journal of Hydrometeorology* **5**: 325–340.

Lundquist JD, Neiman PJ, Martner B, White AB, Gottas DJ, Ralph FM. 2008. Rain versus Snow in the Sierra Nevada, California: comparing radar and surface observations of melting level. *Journal of Hydrometeorology* **9**: 194–211.

Mann HB. 1945. Non-parametric tests against trend. *Econometrica* **13**: 245–259.

Mann HB, Whitney DR. 1947. On a test of whether one of two random variables is stochastically larger than the other. *Annals of Mathematical Statistics* **18**(1): 50–60.

Manning MR, Edmonds J, Emori S, Grubler A, Hibbard K, Joos F, Kainuma M, Keeling RF, Kram T, Manning AC, Meinshausen M, Moss R, Nakicenovic N, Riahi K, Rose SK, Smith S, Swart R, van Vuuren DP. 2010. Misrepresentation of the IPCC CO2 emission scenarios. *Nature Geoscience* **3**: 376–377 doi:10.1038/ngeo880.

Maraun D, Wetterhall F, Ireson AM, Chandler RE, Kendon EJ, Widmann M, Brienen S, Rust HW, Sauter T, Thermeßl M, Venema VKC, Chun KP, Goodess CM, Jones RG, Onof C, Vrac M, Thiele-Eich I. 2010. Precipitation downscaling under climate change: recent developments to bridge the gap between dynamical models and the end user. *Reviews of Geophysics* **48**, RG3003, doi:10.0000/8755-1209/10/2009RG000314.

Marks D, Dozier J. 1992. Climate and energy exchange at the snow surface in the alpine region of the Sierra-Nevada. 2. Snow cover energy balance. *Water Resources Research* **28**(11): 3043–3054.

Maurer EP. 2007. Uncertainty in hydrologic impacts of climate change in the Sierra Nevada, California, under two emission scenarios. *Climatic Change* **82**: 309–325.

Meehl GA, Washington WM, Wigley TML, Arblaster JM, Dai A. 2003. Solar and greenhouse gas forcing and climate response in the twentieth century. *Journal of Climate* **16**: 426–444.

Minder JR, Mote PW, Lundquist JD. 2010. Surface temperature lapse rates over complex terrain: lessons from the Cascade Mountains. *Journal of Geophysical Research* **115**: D14122, doi:10.1029/2009JD013493.

Murray CD, Buttle JM. 2003. Impacts of clearcut harvesting on snow accumulation and melt in a northern hardwood forest. *Journal of Hydrology* **271**: 197–212.

Nash JE, Sutcliffe JV. 1970. River flow forecasting through conceptual models. Part I – a discussion of principles. *Journal of Hydrology* **10**(3): 282–290.

Null SE, Viers JH, Mount JF. 2010. Hydrologic response and watershed sensitivity to climate warming in California's Sierra Nevada. *PLoS One* **5**: e9932. doi:10.1371/journal.pone.0009932.

Pomeroy JW, Marks D, Link T, Ellis C, Hardy J, Rowlands A, Granger R. 2009. The impact of coniferous forest temperature on incoming longwave radiation to melting snow. *Hydrological Processes* **23**: 2513–2525 doi:10.1002/hyp. 7325.

Rantz SE et al.1982. Measurement and computation of streamflow: volume 1. Measurement of stage and discharge, U.S. Geological Survey Water-Supply Paper 2175, U.S. Dept. of the Interior, Washington, D. C.; 284.

Regonda S, Rajagopalan B, Clark M, Pitlick J.2005. Seasonal cycle shifts in hydroclimatology over the Western US. *Journal of Climate* **18**: 372–384.

Rice R, Bales RC, Painter TH, Dozier J. 2011. Snow water equivalent along elevation gradients in the Merced and Tuolumne River basins of the Sierra Nevada. *Water Resources Research* **47**, W08515, doi:10.1029/2010WR009278.

Robinson M, Cognard-Plancq AL, Cosandey C, David J, Durand P, Fuhrer HW, Hall R, Hendriques MO, Marc V, McCarthy R, McDonnell M, Martin C, Nisbet T, O'Dea PO, Rodgers M, Zollner A. 2003. Studies of the impact of forests on peak flows and baseflows: a European perspective. *Forest Ecology and Management* **186**: 85–97.

Running S, Nemani R, Hungerford R.1987. Extrapolation of synoptic meteorological data in mountainous terrain and its use for simulating forest evapotranspiration and photosynthesis. *Canadian Journal of Forest Research* **17**: 472–483.

Safeeq M, Fares A. 2011. Hydrologic response of a Hawaiian watershed to future climate change scenarios. *Hydrological Process* doi: 10.1002/hyp.8328.

Schnorbus MA, Alila Y. 2004. Forest harvesting impacts on the peak flow regime in the Columbia Mountains of southeastern British Columbia: an investigation using long-term numerical modeling. *Water Resources Research* **40**, doi:10.1029/2003WR002918.

Sen PK. 1968. Estimates of the regression coefficient based on Kendall's tau. *Journal of the American Statistical Association* **63**: 1379–1389.

Shuttleworth J. 1992. Evaporation. *Chapter 4 of the Handbook of Hydrology*, Maidment D (ed). McGraw-Hill, Inc.: New York.

Sicart JE, Pomeroy JW, Essery RLH, Hardy J, Link T, Marks D. 2004. A sensitivity study of daytime net radiation during snowmelt to forest canopy and atmospheric conditions. *Journal of Hydrometeorology* **5**: 774–784.

Stewart I, Cayan DR, Dettinger MD. 2005. Changes towards earlier streamflow timing across western North America. *Journal of Climate* **18**: 1136–1155.

Storck P. 2000. Trees, snow and flooding. An investigation of forest canopy effects on snow accumulation and melt at the plot and watershed scales in the Pacific Northwest. In: Water Resources Series, Technical Report 161. University of Washington, Seattle, WA; 176 .

Storck P, Lettenmaier DP, Bolton SM. 2002. Measurement of snow interception and canopy effects on snow accumulation and melt in a mountainous maritime climate, Oregon, United States. *Water Resources Research* **38**: 1–16.

Stouffer RJ, Broccoli AJ, Delworth TL, Dixon KW, Gudgel R, Held I, Hemler R, Knutson T, Lee H-C, Schwarzkopf MD, Soden B, Spelman MJ, Winton M, Zeng F. 2006. GFDL's CM2 global coupled climate models – part 4: idealized climate response. *Journal of Climate* **19**: 723–740.

Strasser U, Warscher M, Liston GE. 2011: Modeling snow–canopy processes on an idealized mountain. *Journal of Hydrometeorology* **12**: 663–677, doi: 10.1175/2011JHM1344.1.

Tague C, Seaby A, Hope A. 2008. Modeling the eco-hydrologic response of a Mediterranean type ecosystem to the combined impacts of projected climate change and altered fire frequencies. *Climatic Change* **93**: 137–155 DOI: 10.1007/s10584-008-9497-7.

Teng J, Vaze J, Chiew FHS, Wang B, Jean-Michel Perraud J-M.2012. Estimating the relative uncertainties sourced from GCMs and hydrological models in modelling climate change impact on runoff. *Journal of Hydrometeorology* **13**: 122–139 doi: 10.1175/JHM-D-11-058.1.

Theil H. 1950a. A rank-invariant method of linear and polynomial regression analysis. *I. Proceedings of the Koninklijke Nederlandse Akademie van Wetenschappen (KNAW)* **53**:386–392.

Theil H. 1950b. A rank-invariant method of linear and polynomial regression analysis. *II. Proceedings of the Koninklijke Nederlandse Akademie van Wetenschappen (KNAW)* **53**: 521–525.

Theil H. 1950c. A rank-invariant method of linear and polynomial regression analysis. *III. Proceedings of the Koninklijke Nederlandse Akademie van Wetenschappen (KNAW)* **53**: 1397–1412.

Thyer M, Beckers J, Spittlehouse D, Alila Y, Winkler R. 2004. Diagnosing a distributed hydrologic model for two high-elevation forested catchments based on detailed stand- and basin-scale data. *Water Resources Research* **40**, 1.doi:10.1029/2003WR002414.

U.S. Department of Agriculture, Natural Resources Conservation Service. 2006. Soil Survey Geographic (SSURGO) database for Yosemite National Park, California, ca790. Available at: http://SoilDataMart.nrcs.usda.gov/

Varhola A, Coops NC, Weiler M, Moore RD. 2010. Forest canopy effects on snow accumulation and ablation: an integrative review of empirical results. *Journal of Hydrology* **392**(3–4): 219–233, doi:10.1016/j.jhydrol.2010.08.009.

Veatch W, Brooks PD, Gustafson JR, Molotch NP. 2009. Quantifying the effects of forest canopy cover on net snow accumulation at a continental, mid-latitude site. *Ecohydrology* **2**: 115–128.

Waichler SR, Wigmosta MS. 2003. Development of hourly meteorological values from daily data and significance to hydrological modeling at H. J. Andrews Experimental Forest. *Journal of Hydrometeorology* **4**: 251–263.

Washington WM, Weatherly JW, Meehl GA, Semtner AJ, Bettge TW, Craig AP, Strand WG, Arblaster J, Wayland VB, James R, Zhang Y. 2000. Parallel climate model (PCM) control and transient simulations. *Climate Dynamics* **16**: 755–774.

Whitaker A, Alila Y, Beckers J. 2002. Evaluating peak flow sensitivity to clear-cutting in different elevation bands of a snowmelt dominated mountainous catchment. *Water Resources Research* **38**(9): 1172, doi:10.1029/2001WR000514.

Whitaker A, Alila Y, Beckers J, Toews D. 2003. Application of the distributed hydrology soil vegetation model to Redfish Creek, British Columbia: model evaluation using internal catchment data. *Hydrol. Process.* **17**: 199–224, doi:10.1002/hyp.1119.

Wigley TML. 2009. The effect of changing climate on the frequency of absolute extreme events. *Climatic Change* **97**: 67–76, DOI 10.1007/s10584-009-9654-7.

Wigmosta MS, Vail LW, Lettenmaier DP. 1994. A distributed hydrology-vegetation model for complex terrain. *Water Resources Research* **30**: 1665–1679.

Wigmosta MS, Nijssen B, Storck P, Lettenmaier DP. 2002. The distributed hydrology soil vegetation model. In *Mathematical Models of Small Watershed Hydrology and Applications*, Singh VP, Frevert DK. (eds). Water Resource Publications: Littleton, CO; 7–42.

Wilcoxon F. 1945. Individual comparisons by ranking methods. *Biometrics Bulletin* **1**(6): 80–83.

Wiley MW, Palmer RN. 2008. Estimating the impacts and uncertainty of climate change on a municipal water supply system. *Journal of Water Resources Planning and Management* **134**: 239–246, DOI: 10.1061/(ASCE)0733-9496(2008)134:3(239).

Winkler RD. 2011.Changes in snow accumulation and ablation after a fire in south-central British Columbia. *Streamline Watershed Management Bulletin* **14**: 1–7.

Winkler RD, Spittlehouse DL, Golding DL. 2005. Measured differences in snow accumulation and melt among clearcut, juvenile, and mature forests in Southern British Columbia. *Hydrological Processes* **9**:51–62.

Winstral AH, Marks, DG, Gurney R. 2009. An efficient method for distributing wind speeds over heterogeneous terrain. *Hydrological Processes* **23**(17): 2526–2535.

Winstral A, Elder K, Davis RE. 2002. Spatial snow modeling of wind-redistributed snow using terrain-based parameters. *Journal of Hydrometeorology* **3**(5): 524–538.

Yue S, Hashino M. 2003. Temperature trends in Japan: 1900–1996. *Theoretical and Applied Climatology* **75**: 15–27.

Yue S, Pilon P, Phinney B, Cavadias G. 2002. The influence of autocorrelation on the ability to detect trend in hydrological series. *Hydrological Processes* **16**(9): 1807–1829, DOI: 10.1002/hyp.1095.

Zhao Q, Liu Z, Ye B, Qin Y, Wei Z, Fang S. 2009. A snowmelt runoff forecasting model coupling WRF and DHSVM. *Hydrology and Earth System Sciences* **13**: 1897–1906.

APPENDIX A: A1. DESCRIPTION OF SNOWPACK ENERGY BALANCE

The snow pack energy balance equation and its components are described in Wigmosta *et al.* (1994). The snowpack energy balance equation implemented in DHSVM is based on the following formulation:

$$c_s SWE \frac{dT_s}{dt} = R_{ns} + Q_s + Q_l + Q_p + Q_m \tag{A1}$$

where c_s is the ice-specific heat, SWE is the snowpack water equivalent, T_s is the temperature of the snowpack, t is time, R_{ns} is the net radiation, Q_s is the sensible heat, Q_l is the gained latent heat from condensation or lost to sublimation, Q_p is the advected heat to the snowpack from rainfall and Q_m is the internal latent heat gained from refreezing of liquid water for T_s below 0 °C or lost by melting for T_s above 0 °C. Equation (A1) is solved through a finite difference scheme. If T_s reaches 0 °C during the computational time step, Q_m is the melt energy calculated as follows:

$$Q_m = R_{ns} + Q_s + Q_l + Q_p + c_s SWE \cdot T_s^t \tag{A2}$$

where T_s^t is the snowpack temperature at the beginning of the time step t.

Net radiation R_{ns} is composed of the net shortwave radiation R_{ss} and the net longwave radiation R_{ls}:

$$R_{ns} = R_{ss} + R_{ls} \tag{A3}$$

The amount of shortwave radiation R_{ss} at the snow surface is estimated on the basis of the total amount of incident solar radiation R_s and the filtering effects from the canopy as

$$R_{ss} = R_s(1 - \alpha_s)(\tau_o F + (1 - F)) \tag{A4}$$

where α_s is the snow reflection coefficient (albedo), F is the forest fractional cover and τ_o is the fraction of R_s transmitted by the overstory canopy, calculated on the basis of a form of Beer's law as

$$\tau_o = \exp(-kLAI_o) \tag{A5}$$

where k is canopy attenuation coefficient and LAI_o is the overstory LAI.

In the absence of site-specific albedo data, the curves modelling albedo in the Tuolumne area were parameterized identically for both barren and forested areas. Separate decay functions were used for below and above freezing conditions, driven by the simulated surface temperature T_{ss}, with albedo decreasing more rapidly during melting, based on the following equations:

Forest Subfreezing :

$$\alpha_s = \alpha_0 * 0.92^{(d)^{0.58}}, \quad minimum\ 0.7, T_{ss} < 0\ ^\circ\mathrm{C} \tag{A6}$$

Forest Melting :

$$\alpha_s = \alpha_0 * 0.87^{(d)^{0.46}}, \quad minimum\ 0.5, T_{ss} > 0\ ^\circ\mathrm{C} \tag{A7}$$

where α_0 is set to 0.85, the albedo of fresh snow, d is the number of days since the last snowfall.

The net longwave radiation R_{ls} is estimated as follows:

$$R_{ls} = L_o F + (L_d(1 - F)) - L_s \tag{A8}$$

in which L_d is incoming longwave radiation, L_0 is the upward overstory longwave radiation flux and L_s is the upward longwave radiation from the snow surface. Both L_0 and L_s are given by similar expressions of the following form:

$$L_o = \sigma(T_0 + 273)^4 \text{ and } L_s = \sigma(T_s + 273)^4 \tag{A9}$$

in which T_0 is the overstory temperature and σ is the Stefan–Boltzman constant.

The sensible heat flux Q_s is estimated as follows:

$$Q_s = \frac{\rho c_p (T_a - T_s)}{r_{as}} \tag{A10}$$

where ρ is the density of air, c_p is the specific heat of air, T_a is the air temperature and r_{as} is the surface resistance corrected for atmospheric stability and vegetation effects.

The latent heat term Q_e in the energy balance equation is given by the following:

$$Q_e = \frac{\lambda_i \rho \left(\frac{0.622}{P_a}\right)(e(T_a) - e_s(T_s))}{r_{as}} \tag{A11}$$

in which λ_i represents either the latent heat of vapourization during melting conditions or the latent heat of fusion during freezing conditions, P_a is the atmospheric pressure, and e and e_s are the vapour pressures at T_a and T_s, respectively.

Q_p, the advected heat to the snowpack from rainfall, is

$$Q_p = \rho_w c_w T_p(P_r) \tag{A12}$$

where ρ_w is the density of water, c_w is the specific heat of water, T_p is the temperature of precipitation, assumed equal to the air temperature T_a, and P_r is precipitation as rain.

Finally, the internal latent heat gained from melting or refreezing for snow surface temperatures different than 0 °C is calculated as follows:

$$Q_m = \lambda_i \rho_w M \quad \text{(A13)}$$

where M is the depth of snowmelt (negative flux) or the volume of refrozen liquid water (positive flux).

DHSVM code, additional documentation and pre-processing and post-processing tools are available to download at http://www.hydro.washington.edu/Lettenmaier/Models/DHSVM/index.shtml

References listed in Table A1 are as follows: R1: NPS vegetation survey data; R2: Thyer *et al*. (2004); R3: Storck (2000); R4: Whitaker *et al.* (2003), R5: Bewley *et al*. (2010), R6: Zhao *et al*. (2009), R7: ranges provided in Carsel and Parrish (1988) based on USDA soil classifications (USDA NRCS 2006), R8: Andreadis *et al*. (2009); and R9: Lundquist *et al*. (2008).

A2. DHSVM MODEL SET-UP AND SENSITIVITY TESTS

Radiation attenuation by the canopy was a sensitive parameter influencing the modelled timing of streamflow. Parameterizations of the albedo curves, also part of the shortwave radiation model (Equations (A6) and (A7),

Table A1. DHSVM parameters used for the upper Tuolumne area, Sierra Nevada

	Value	References
Forest parameters		
Overstory vegetation height (m)	13.6	R1
Understory vegetation height (m)	0.5	R1
Overstory fractional coverage (%)	80	R1
Understory fractional coverage (%)	80	R1
Overstory leaf area index, LAI (−)	5.0	R1
Understory leaf area index, LAI (−)	3.0	R1
Radiation attenuation	0.3	R2
Maximum snow interception capacity (m SWE)	0.02	R2
Snow interception efficiency (−)	0.6	R3
Mass release drip ratio	0.4	R3
Minimum melt needed for mass release (m SWE)	0.002	R3
Snow mass release/drip ratio (−)	0.4	R3
LAI multiplier for rain (m)	0.0001	R4
LAI multiplier for snow (m)	0.005	R5
Aerodynamic attenuation coefficient	2.0	R4
Maximum stomatal resistance (sm^{-1}) overstory	5000	R6
Maximum stomatal resistance (sm^{-1}) understory	3000	R6
Minimum stomatal resistance (sm^{-1}) overstory	650	R6
Minimum stomatal resistance (sm^{-1}) understory	200	R6
Vapour pressure deficit causing stomatal closure overstory (Pa)	4000	R2
Vapour pressure deficit causing stomatal closure understory (Pa)	4000	R2
Moisture threshold below which transpiration is restricted overstory (−)	0.33	R4
Moisture threshold below which transpiration is restricted understory (−)	0.13	R4
Albedo	0.2	R6
Overstory root fractions in soil layers 1–3	0.2; 0.4; 0.4;	R6
Understory root fractions in soil layers 1–3	0.4; 0.6; 0.0;	R6
Soil parameters		
Sand		
Lateral saturated hydraulic conductivity K_{lat} ($m\,s^{-1}$), porosity (−)	8.2e−5; 0.43	R7
Loamy sand		
Lateral saturated hydraulic conductivity K_{lat} ($m\,s^{-1}$), porosity (−)	4.05e−5; 0.42	R7
Sandy loam		
Lateral saturated hydraulic conductivity K_{lat} ($m\,s^{-1}$), porosity (−)	1.3e−5; 0.4	R7
Bedrock		
Lateral saturated hydraulic conductivity K_{lat} ($m\,s^{-1}$), porosity (−)	1.0e−8; 0.4	R7
Other parameters		
Snow roughness (m)	0.01	R8
Minimum air temperature for snow (°C)	3.0	R9
Minimum air temperature for rain(°C)	0.0	R9

Appendix A), were found in other studies to influence the modelled SWE under the forest (Thyer *et al*., 2004; Jost *et al*., 2009; Bewley *et al*., 2010). However, albedo observations under the forest canopy were not available in the Tuolumne basin; therefore, model default albedo functions were used in model simulations (Equations (A6) and (A7), Appendix A). The remaining final DHSVM calibration parameters are listed in Table A1.

Daily climate data were disaggregated into 3-hourly values using the existing pre-processing tools accompanying DHSVM, in which few adjustments were made specific to this project. Within these algorithms, the following assumptions were included. Precipitation was distributed uniformly throughout the day. Diurnal temperature variations were established on the basis of the daily extremes from the climate data and the site location for estimating the approximate times of the day when these extremes are likely to occur. The daily minimum and maximum temperatures were then interpolated for 3-hourly variations using hermite polynomials. The maximum relative humidity was assumed to occur at the minimum air temperature, which was taken equal to the dew point temperature. Diurnal relative humidity fluctuations were then established on the basis of the ratios of vapour pressures at a given temperature during the day and the vapour pressure at the minimum temperature based on a model by Running *et al*. (1987). The 3-hourly solar radiation series was generated using an algorithm proposed by Bristow and Campbell (1984), which was calibrated to best match the hourly rates recorded at Dana Meadows during the 2003–2009 period. Incoming longwave radiation was generated using the Idso (1981) method. For each day of the year, the 3-hourly wind speed values were assumed to be equal to the daily average wind speed recorded at Dana Meadows during the 2003–2009 period. The 2001–2003 period was used for spin-up simulations.

We assessed the uncertainty of the most sensitive forest parameters and their effects on model response when temperature increases. These additional tests were considered because direct measurements of snow under the forest were not available for the 2003–2009 calibration period, and therefore, direct comparisons of the simulated and observed SWE under the forest were not possible. However, the forest effects at the basin scale were explicitly taken into account through distributed modelling and canopy parameterization, as described in the Hydrologic Model Description and Model Set-up Section, and through model calibration on the streamflow data as the model integrated response. Alila and Beckers (2001) identified the most sensitive forest parameters for snow accumulation and melt in DHSVM as the fractional cover (F), LAI, radiation attenuation (k) and wind (aerodynamic) attenuation (a).

During preliminary runs, we tested k, LAI and a for the historic 2003–2009 meteorology. The base parameters were $k = 0.3$, LAI = 5.0 and $a = 2.0$, respectively established during calibration (Appendix A, Table A1). These values were varied sequentially from $k = 0.1$ to $k = 0.5$ (for k), LAI = 3.0 to LAI = 7.0 (for LAI), and $a = 1.0$ to $a = 3.0$ (for a), while holding all the remaining parameters constant. These tested parameters influenced the simulated SWE more significantly during the melt season than during the accumulation season, with patterns of SWE sensitivity similar to those shown in Figure 4 in Alila and Beckers, 2001. Fractional cover was not part of these preliminary tests, as its sensitivity was previously considered within the vegetation scenarios in the climate change model runs (Table II). Because SWE during the melt period was most sensitive to the radiation attenuation k, we chose this parameter to further illustrate the uncertainty in forest parameterization in the historic T and historic $T + 3\,^{\circ}\mathrm{C}$ temperature scenarios. The calibration k was set to 0.3, corresponding to a value of τ_o, the fraction of incoming solar radiation R_s transmitted by the canopy (Equation (A5), Appendix A), of 0.22. The k value was subsequently ranged from 0.1 ($\tau_o = 0.60$) to 0.5 ($\tau_o = 0.08$), the same levels of sensitivity used in Alila and Beckers (2001) (scenarios 1–4, TableA2).

The results from this sensitivity analysis are illustrated in Figure A1b,d,f,h that show the simulated SWE at Dana Meadows (Figure 10b,d) and Tuolumne Meadows (Figure 10f,h) as a result of varying k, the radiation attenuation coefficient, corresponding to fractions transmitted of 0.60 ($k = 0.1$), 0.22 ($k = 0.3$, calibration value) and 0.08 ($k = 0.5$) for the two temperature scenarios. Examination of Figure 10b,d,f,h leads to two observations: (i) the snowpack under the forest melted earlier in the increased temperature scenario than the snowpack on bare ground even considering the relatively large uncertainty in shortwave radiation parameterization (Figure 10d,h) and (ii) the sensitivity of simulated SWE to k during the melting season decreases when temperature increases (Figure 10b,d,f,h). This effect is more apparent at the lower elevation snow pillow site, Tuolumne Meadows, than at the higher elevation site, Dana Meadows (Figure 10d,h). The variations in k were also reflected in the simulated hydrograph (Figure 10a,c, e,g). Assuming $k = 0.3$ (calibration value), in the historic T scenario, the forest COM occurred 9 days earlier than the barren COM (Figure 10a). This difference increased to 26 days for $k = 0.1$, whereas for $k = 0.5$, the forest COM occurred 12 days later than the barren COM (Figure 10a,c). In the increased temperature scenario, forest COM occurred earlier than barren COM by 32

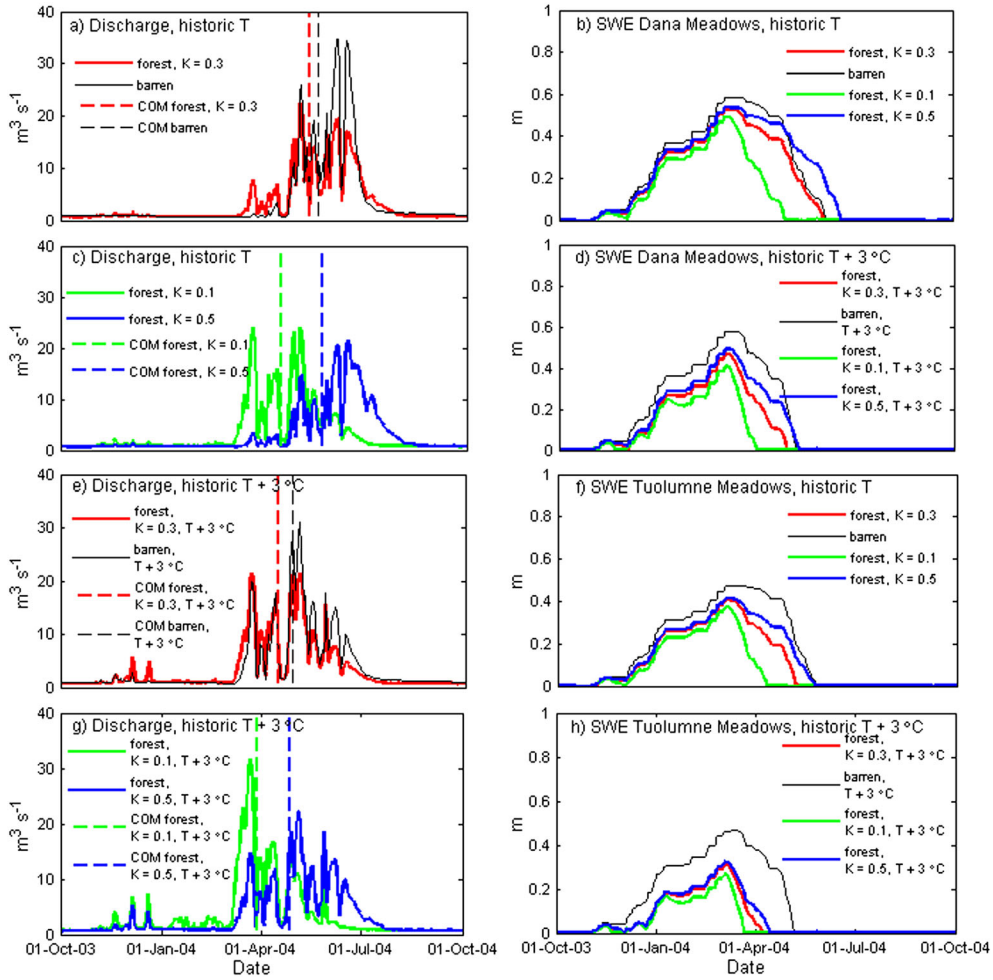

Figure A1. a), c), e), g) Simulated daily hydrographs assuming historic and increased air temperatures for barren scenario and for uniform forest scenario with variable radiation attenuation parameter k; b), d), f), h) SWE levels for the same scenarios at Dana Meadows and Tuolumne Meadows locations. Vertical lines identify COM for each hydrograph. All plots are shown for water year 2004

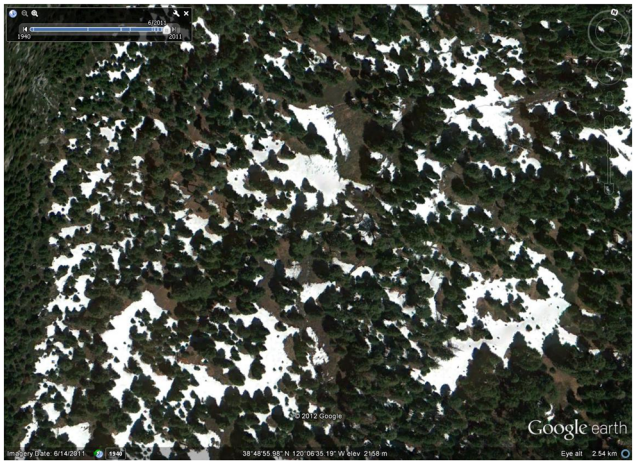

Figure A2. Google Earth 6.2.image (June 14, 2011) approximately 124.2 km from the Tuolumne Meadows in the Sierra Nevada centred at 38°48′56″N, 120°06′35″W and 2158 m elevation, showing snow lasting longer in the barren areas than under the forest. Available through http://www.google.com/earth/index.html [Accessed June 2012]

($k = 0.1$), 14 ($k = 0.3$) and 3 days ($k = 0.5$), respectively. Figure A2 shows a snow-covered landscape in the spring of 2011 in the Sierra Nevada north of the Tuolumne area (38°48′56″, 120°06′35″). The snow under the forest has largely disappeared, whereas snow remains in the barren areas.

Table A2. DHSVM scenarios for radiation attenuation sensitivity tests

Scenario	Vegetation cover	Scenario assumption
1	Current forest	$k = 0.1$ ($\tau_o = 0.60$), historic T
2	Current forest	$k = 0.5$ ($\tau_o = 0.08$), historic T
3	Current forest	$k = 0.1$ ($\tau_o = 0.60$), historic $T + 3$°C
4	Current forest	$k = 0.5$ ($\tau_o = 0.08$), historic $T + 3$°C